JGR Atmospheres

RESEARCH ARTICLE
10.1029/2023JD040681

Observation of Electrical Alignment Signatures in an Isolated Thunderstorm by Dual-Polarized Phased Array Weather Radar and the Relationship With Intracloud Lightning Flash Rate

Shuo Wang[1], Yuuki Wada[1], Syugo Hayashi[2], Tomoo Ushio[1], and V. Chandrasekar[3]

[1]Osaka University, Suita, Japan, [2]Meteorological Research Institute, Japan Meteorological Agency, Tsukuba, Japan, [3]Colorado State University, Fort Collins, CO, USA

Key Points:

- The composite K_{DP} could be used as an indicator of intracloud (IC) lightning potential in isolated thunderstorms
- The negative K_{DP} volume and average composite K_{DP} show well correlations with the IC lightning flash rate in an isolated thunderstorm
- The vertical structure of total electric field in the upper parts of an isolated thunderstorm could be explored by negative K_{DP} signatures

Correspondence to:
S. Wang,
wang@se.eei.eng.osaka-u.ac.jp

Citation:
Wang, S., Wada, Y., Hayashi, S., Ushio, T., & Chandrasekar, V. (2024). Observation of electrical alignment signatures in an isolated thunderstorm by dual-polarized phased array weather radar and the relationship with intracloud lightning flash rate. *Journal of Geophysical Research: Atmospheres*, *129*, e2023JD040681. https://doi.org/10.1029/2023JD040681

Received 25 DEC 2023
Accepted 11 SEP 2024

Author Contributions:
Conceptualization: Shuo Wang, Tomoo Ushio, V. Chandrasekar
Data curation: Syugo Hayashi
Funding acquisition: Tomoo Ushio
Investigation: Yuuki Wada, Syugo Hayashi
Methodology: Shuo Wang
Project administration: Tomoo Ushio
Software: Shuo Wang
Supervision: Tomoo Ushio
Validation: Yuuki Wada
Writing – original draft: Shuo Wang
Writing – review & editing: Yuuki Wada, Syugo Hayashi, Tomoo Ushio, V. Chandrasekar

Abstract The electrical alignment signatures of ice crystals in the middle and upper parts of a thunderstorm have a physical connection with the strong electric fields within the cloud. By taking advantage of the high spatio-temporal resolution of an X-band dual-polarized multiparameter phased array radar, this paper employs negative K_{DP} signatures to investigate the variation of electric fields in an isolated thunderstorm within its evolution, and the relationship between the negative K_{DP} signatures and intracloud (IC) lightning activity. The results show that the radar-inferred strong electric fields distributed in a region of about 8.5–10 km during the developing stage, then extended from about 10 km to the cloud top during the mature stage, with an increasing IC lightning flash rate before the end of the mature stage. Subsequently, the electric fields weakened associated with a large amount of IC lightning discharges. The qualitative analysis results indicate that the evolution of the radar-inferred electric fields associated with the upper charge regions is consistent with the electrification process in the isolated thunderstorm, inferred by the IC lighting activity. In addition, there is a tendency for the increased IC lightning rate as the decrease in average composite K_{DP} in the middle and upper layers of the thunderstorm, with a time lag of about 5.5 min between the minimum average composite K_{DP} and the peak IC lightning rate, while a good correlation between the negative K_{DP} volume and the IC lightning flash rate at a lag of approximately 9 min.

Plain Language Summary By using an X-band dual-polarized multiparameter phased array radar with high temporal and spatial resolution, this study investigates the electrical alignment signatures of ice particles related to the strong electric fields in the middle and upper parts of an isolated thunderstorm. The results indicate the potential use of electrical alignment signatures of ice crystals for evaluating the evolution of radar-inferred electric fields within the thunderstorm lifecycle. Moreover, well correlations are observed between negative K_{DP} volume, average composite K_{DP}, and intracloud lightning flash rate.

1. Introduction

With the widespread application of weather radar, there are numerous researches explored the relationships between lightning activity and radar-inferred microphysical characteristics and the kinematic structure of thunderstorms, which significantly advanced the exploration of the evolution of the cloud electrification process and the utilization of weather radar for the monitoring of severe thunderstorms, issuing early warnings, and the prediction of lightning activity.

The earliest research with the observation by weather radar explored the properties of lightning activity and the charge structure associated with the vertical structure of reflectivity within the development of precipitation regions. Workman and Reynolds (1949) and Reynolds and Brook (1956) studied the initial electrification with the initial radar precipitation echo and the top height of the radar echo by an airborne weather radar. The results showed that the ice phase hydrometeors within the updraft correlated well with the initial electrification, and the electrification was probably initiated in a region with a temperature of about −10°C in New Mexico. Dye et al. (1988) used ground-based Doppler weather radar to observe small thunderstorms in New Mexico and showed that the negative charge region was located in the region of reflectivity from 25 to 30 dBZ. With more cases in New Mexico thunderstorms (Dye et al., 1989), they found that the reflectivity around 40 dBZ at or above the −10°C layer appeared at the onset of electrification, and concluded that the reflectivity could not be used alone

as a reliable indicator of electrification, which was consistent with the conclusion from Reynolds and Brook (1956) that the precipitation only does not guarantee thunderstorm electrification unless the precipitation experiences rapid vertical development. Considering the important role of updrafts in electrification, the relationships between lightning activity and updrafts have been studied (Lhermitte & Krehbiel, 1979; Shackford, 1960; Williams, 1981, 1985; Zipser & Lutz, 1994). Lhermitte and Krehbiel (1979) suggested that lightning activity increased with increasing maximum reflectivity in the vicinity of the updraft and rapidly increased updraft velocity with a maximum value of larger than 20 m/s within the mixed-phase region. Williams (1981, 1985) studied thunderstorm cases in New Mexico, Florida, and New England, with the observation by vertical scanning radars, and the results showed that the lightning flash rate is strongly related to the echo top height in the cases of electrically active storms. Especially in Florida, the flash rate exhibited a strong correlation with the fifth power of the echo top height except in the decay stage. Zipser and Lutz (1994) proposed that updraft velocities exceeding specific threshold values are crucial for rapid electrification. They suggested the updraft with an average vertical velocity greater than about 6–7 and 10–12 m/s for the maximum vertical velocity within the temperature range of 0 to −20°C. Ushio et al. (2001) examined the power scaling law at different seasons and regions by precipitation radar on the TRMM satellite and concluded that the relationship between storm height and flash rate is non-linear, exhibiting considerable variability, which suggested that using only the echo top height cannot establish a reliable relationship with lightning flash rate.

Due to the dual-polarization weather radar offers additional polarimetric parameters used for hydrometeor classification, estimation of particle size, shape, and orientation, and thermodynamic phase. The capability to differentiate particle types in mixed-phase hydrometeors leads to an improved understanding of the storm microphysics and structure, which is especially helpful for the parameterization of lightning flash rate. A multitude of studies have demonstrated strong correlations between lightning flash rate and thunderstorm microphysics and kinematic parameters, such as the ice (e.g., precipitation, total) mass, graupel volume, updraft volume, and so on (Basarab et al., 2015; Carey & Rutledge, 1996, 1998, 2000; Deierling & Petersen, 2008; Fehr et al., 2005; Goodman et al., 1988; Mecikalski et al., 2015; Tessendorf et al., 2007; Wiens et al., 2005). Goodman et al. (1988) found that the maximum total flash rate corresponded with the maximum in storm mass, 30 dBZ echo volume, vertically integrated liquid water content, and cloud height. Fehr et al. (2005) investigated the relationship between lightning activity and different hydrometeor particle mass inferred by radar observations in three types of thunderstorms, including a multi-cell storm, a supercell storm, and a squall line. The result indicated that, above the −20°C layer, the total mass, graupel mass, and hail mass were correlated well with lightning activity in isolated thunderstorms, while no such relationship was observed in the squall line with many coexisting convective cells. This result suggested that the lightning flash rate could not be parameterized by total mass alone. Deierling and Petersen (2008) suggested that there is a good correlation between the mean total lightning rate and the updraft volume above the −5°C temperature layer with vertical velocities greater than 5 and 10 m/s Basarab et al. (2015) conducted a validation study in 11 Colorado thunderstorms to examine the relationships between lightning flash rate and graupel volume, 35 dBZ echo volume in the mixed-phase region, and non-precipitation ice mass flux. The result showed that the 35 dBZ echo volume exhibited the strongest correlation with the lightning flash rate. In particular, the microphysical properties related to graupel (graupel volume/mass) have been proven to be closely related to lightning flash rate (Calhoun et al., 2013; Carey & Rutledge, 1996, 2000; Carey et al., 2019; Kuhlman et al., 2006; Mecikalski et al., 2015; Tessendorf et al., 2007; Wiens et al., 2005). By observing a multi-cell thunderstorm in Colorado, Carey and Rutledge (1996) corroborated that the graupel volume above the melting layer inferred by weather radar has well relationship with IC lightning flash rate, and the maximum graupel volume appeared before the peak of IC lightning flash rate. Carey and Rutledge (2000), by studying a deep island convection case, showed that the total lightning flash rate was well correlated with the total radar-inferred ice mass and graupel mass in the mixed-phase region (0 to −40°C). By evaluating the performance of early established flash rate parameterization relations in 515 radar volumes of 33 storms, Carey et al. (2019) suggested that the flash rate relation based on graupel volume outperformed all other relations, including those based on graupel mass, 35 dBZ echo volume, and updraft volume. This conclusion further validated the result from Mecikalski et al. (2015) that graupel volume and graupel mass exhibit better correlations with total lightning flash rate than with the updraft parameters based on observation of a single thunderstorm occurred in Alabama. Normally, the presences of graupel are identified by combining horizontal reflectivity (Z_H) with polarimetric parameters such as differential reflectivity (Z_{DR}), specific differential phase shift (K_{DP}), co-polar correlation coefficient (ρ_{HV}), linear depolarization ratio, and environmental temperature data, or by using hydrometeor classification algorithms based on empirical or/and theoretical simulation results of different hydrometeor

particles. For instance, high reflectivity (Z_H > 45 dBZ) combined with low Z_{DR} (Z_{DR} < 0.5 dB) above the melting layer indicates the presence of graupel (Goodman et al., 1988). Alternatively, above the melting layer, lower Z_{DR} (−0.5 to 0.5 dB) with moderate Z_H (40 to 50 dBZ), combined with K_{DP} (−0.5 to 0.5°/km) and ρ_{HV} greater than 0.99, indicate graupel, while lower Z_{DR} (−0.5–1 dB) with large Z_H (50 to 60 dBZ) below the melting layer (Carey & Rutledge, 1996). Basarab et al. (2015) calculated the graupel volume/mass by using the results of graupel and hail identified by a fuzzy logic hydrometeor identification algorithm (HID) developed by Dolan et al. (2013). Carey et al. (2019) and Mecikalski et al. (2015) employed the National Center for Atmospheric Research fuzzy logic Particle IDentification algorithm (PID) (Deierling et al., 2008; Vivekanandan et al., 1999) to calculate graupel volume by using the category of "graupel/small hail" in a region of −5 to −40°C and −10 to −40°C, respectively.

The strong correlations between lightning activity and graupel content, along with the developmental characteristics of ice particles in the mixed-phase region during thunderstorm electrification as illustrated by these studies, are consistent with the principles of the non-inductive charging theory. Except for the graupel volume/mass (or precipitation ice) methods, the total ice volume/mass methods calculate the volume/mass including ice crystals, aggregates, and graupel. Meanwhile, the 35 dBZ volume scheme evaluates the volume typically associated with large precipitation particles in the mixed-phase region, such as graupel and supercooled drops with updrafts (Basarab et al., 2015; Carey et al., 2019). Notably, by discriminating the ice-related particles and raindrops, Hayashi et al. (2021) investigated the relationship between the 35 dBZ volume of ice-related particles and lightning flash rate within 10 isolated thunderstorms, the results showed that the 35 dBZ volume of ice-related particles has a higher correlation with IC and CG lightning flash rates compared with the 35 dBZ volume in the mixed-phase region. It indicates that a better relationship could be obtained by excluding hydrometeors not involved in the non-inductive charging process, such as rain-related droplets, from the radar reflectivity volume.

According to the non-inductive charge-separation mechanism, charges transfer occur during collision between graupel pellets and ice crystals within updrafts in mixed-phase region of thunderstorms, leading to the buildup of charge regions with different polarity in thunderclouds which the sign and magnitude of the charge associated with graupel depend on factors such as temperature, liquid water content, rime accretion rate (Reynolds et al., 1957; Saunders et al., 1991; Takahashi, 1978). Graupel and ice crystals are typically the principal charge carriers responsible for the establishment of charge regions within thunderstorms. However, compared to graupel, only a few studies have investigated the relationship between radar-inferred properties of ice crystals and lightning flash rate, although ice crystals predominantly compose the upper charge regions within thunderstorms.

Ice crystal contents (e.g., concentration, mass) have been proven to have well correlation with lighting flash rate by modeling, satellite and ground-based polarimetric weather radar observational studies (Baker et al., 1995, 1999; Deierling et al., 2005, 2006, 2008; Latham et al., 2007). Deierling et al. (2008) estimated the non-precipitation (major component: aggregates, ice crystals) and precipitation ice (major component: graupel, small hail) mass above the melting layer in 11 storm cases by dual-Doppler polarimetric radar, and suggested that non-precipitation ice mass also has a high correlation with total lightning activity. Notably, the estimation of the non-precipitating ice mass in thunderstorm adopted a method that calculated the ice crystal contents that reflectivity values were below 20 dBZ in the divergence area, due to the ice crystals being hard to detect by radar when mixed with the larger ice particles (e.g., graupel, hails) in updraft area.

An important feature of ice crystals in the upper parts of thunderstorms is that they could exhibit a vertical alignment by strong electric fields, and recover to the horizontal alignment following with weakened electric fields due to lightning discharges. The mutual influence of aerodynamic torques, Brownian motion, and electrostatic torque on the orientation of falling ice particles has been well investigated (Cho et al., 1981; Foster & Hallett, 2002, 2008; Hashino et al., 2014; Noel & Sassen, 2005; Sassen, 1980; Saunders & Rimmer, 1999; Weinheimer & Few, 1987). These studies suggest that the vertical alignment of small ice particles is normally caused by an electric field and not affected by turbulence, and the ice crystals attain their natural aerodynamic orientation after times on the order of 10 ms when electrical forces disappear due to weakened electric fields (Cho et al., 1981). Small ice crystals ranging in diameter from 50 μm to 2 mm could be electrically aligned along the direction of the in-cloud electric field with an intensity of 50–120 kV/m (Foster & Hallett, 2002; Hashino et al., 2014; Saunders & Rimmer, 1999; Weinheimer & Few, 1987). Additionally, columns are more easily aligned than plate crystals, while larger plates are difficult to align compared to smaller ones by a strong electric field (Hashino et al., 2014; Weinheimer & Few, 1987).

The depolarized signatures related to electrically aligned ice crystals have been observed and investigated by dual-polarized weather radar in numerous research (Caylor & Chandrasekar, 1996; Hendry & McCormick, 1976; Krehbiel et al., 1992, 1996; Mattos et al., 2016, 2017; McCormick & Hendry, 1979; Metcalf, 1992, 1995; Schvartzman et al., 2022; Scott et al., 2001; Ventura et al., 2013; Zrnić & Ryzhkov, 1999). Caylor and Chandrasekar (1996) first proposed that the K_{DP} can be used to explore the change in the orientation of ice crystals by electric fields in thunderstorms. Before intracloud (IC) lightning discharge, the ice particles are gradually aligned along the direction of an electric field by an accumulated strong electric field, and the K_{DP} gradually decreases to a negative value, associated with a mean oriented angle of the electrically aligned ice particles greater than 45° from horizontal. Then, the K_{DP} rapidly increases following with the lightning discharge, associated with horizontally reoriented ice particles. Moreover, the negative K_{DP} values are dominated by small electrically aligned ice particles when they are mixed with larger ice aggregates or graupel, while their intrinsic Z_{DR} is masked by polarimetrically isotropic ice aggregates or graupel (Carey et al., 2009; Hubbert, Ellis, Chang, Rutledge, & Dixon, 2014, Hubbert, Ellis, Chang, & Liou, 2014; Ryzhkov & Zrnić, 2007). These features make the negative K_{DP} a reliable indicator for identifying electrically aligned ice crystals in the upper parts of thunderstorms, and the period variation in negative K_{DP} signature could be used to investigate the change of local electric field related to IC lightning discharges. However, due to the limited time resolution of mechanical scanning weather radars, it is still a challenge to observe and study the K_{DP} signatures related to electrically aligned ice crystals and their relationship with lightning flash rate during the rapid evolution of thunderstorms using traditional weather radars.

Utilizing the negative K_{DP} signatures of electrically aligned ice particles, which are physically related to the intensity of a strong electric field in-cloud, this paper qualitatively analyzes the characteristics of the radar-inferred electric field in the middle and upper parts of an isolated thunderstorm during its evolution, employing the dual-polarized multiparameter phased-array weather radar (MP-PAWR) with a time resolution of 30 s and range resolution of 75 m. By using average composite K_{DP} and negative K_{DP} volume, the relationships between the negative K_{DP} signatures, the vertical structure of radar-inferred electric fields related to upper charge regions, and the IC lightning flash rate were investigated within the evolution of an isolated thunderstorm in Saitama Prefecture, Japan. The result demonstrates that, by taking advantage of the high spatio-temporal resolution of phased-array dual-polarimetric weather radar, the MP-PAWRs could be used to explore the radar-inferred electrification process associated with the evolution of strong electric fields in the upper parts of the isolated thunderstorm. Section 2 describes the data used in this paper and the analysis methods, while Section 3 presents the observation and analysis results, including the relationships between characteristics related to upper charge regions and IC lightning flash rate. A summary and discussions are shown in Section 4.

2. Data and Methodology

2.1. Lightning Data and IC Lightning Flash Rate Calculation

Lightning data in this paper were obtained by a lightning detection system called LIghtning DEtection Network system (LIDEN) operated by the Japan Meteorological Agency. LIDEN is a two-dimensional lightning detection system that utilizes a combination of VHF array and LF detector to collect interferometric and time-of-arrival (TOA) measurements based on VHF and LF signals, respectively. The system provides information on intracloud (IC) and cloud-to-ground (CG) discharges, including locations and occurrence time of lightning pulses/strokes, and so on (Ishii et al., 2014). Furthermore, IC flash is composed of single or multiple IC lightning pulses, while the multiple IC lightning pulses are classified into the initial IC lightning pulse, the following IC lightning pulses, and the ending IC lightning pulse.

To investigate the relationship between the variation of the total electrical field in the middle and upper parts of the isolated thunderstorm and the IC lightning flash rate, a flash group algorithm is employed to group IC lightning pluses into IC flashes in an analyzed region of the thunderstorm. After synchronizing the UTC of lightning data to the Japan Standard Time (JST) of radar data, the algorithm calculates the azimuth and distance of each IC lightning pulse relative to the radar location by using the MP-PAWR location as the center and the maximum radar detected range as the radius. The single IC lightning pulse occurring in the analyzed region is counted as one IC lightning flash. In the case of multiple IC lightning pulses, each lightning flash must consist of at least two types of IC lightning pulses which could be located outside the analyzed region: the initial IC lightning

pulse and the ending IC lightning pulse. The IC flash group algorithm applies spatial and temporal constraints to group IC lightning pulses. Specifically, the maximum duration of an IC lightning flash is set to be no greater than 1 s, and the spatial range between consecutive IC lightning pulses is limited to 20 km. Additionally, a maximum azimuth interval of 10° is allowed between consecutive IC lightning pulses. The algorithm proceeds by grouping IC lightning pulses according to the sequence of their occurrence times and the IC lightning pulses are assigned to an IC flash if they meet the requirement of the spatial and temporal constraints. In cases where IC lightning pulses cannot be matched to any existing flash, the spatial range and azimuth interval thresholds are adjusted iteratively until suitable matches are found, and the pulses are grouped as an IC lightning flash.

Due to the two-dimensional location information (latitude and longitude) provided by the LIDEN system for IC lightning pulses, the flash group algorithm utilized in this study may encounter limitations in accurately grouping lightning pulses into IC lightning discharges, particularly when multiple IC lightning pulses occur within the same spatial range during the maximum flash duration. However, since this paper mainly examines the relationship between IC lightning flash rate and the electrical alignment signatures observed by MP-PAWR in isolated thunderstorms, it is still feasible to calculate the IC lightning flash rate to compare the trends of flash rate with the evolution of the electric fields in the isolated thunderstorm.

2.2. Radar Data and Quality Control

In this paper, the polarimetric radar data were collected by an X-band dual-polarized phased-array weather radar (MP-PAWR) developed by Toshiba Corporation, Osaka University, and the National Institute of Communication and Technology (NICT), which is located at an altitude of 29.3 m above sea level at Saitama University (35.86158°N, 139.60908°E). With an electronically scanned beam width in the elevation direction of less than 1° and an elevation angle increment of less than 1° within elevation angles of 0–90°, MP-PAWR performs a volume scan with 114 elevations at a temporal resolution of 30 s by operating in its normal operational mode, while the range resolution is 75 m within the maximum detected range of 60 km. With the high spatio-temporal resolution along with its fast and flexible scanning capability, the MP-PAWR could perform a simultaneous and continuous observation of the mixed-phase region during the thunderstorm evolution, thereby offering valuable information to study the evolution of cloud electrification throughout the entire lifecycle of thunderstorms.

To investigate the relationship between the lightning activity and the electrical-related characteristics associated with the upper charge regions inferred by phased array weather radar, an isolated thunderstorm on 20 August 2019 is selected for analysis. Before analysis, radar data quality control is applied on polarized parameters of MP-PAWR, including the horizontal reflectivity Z_H, differential propagation phase shift (Φ_{DP}), and K_{DP} (Wang et al., 2024). Considering that depolarized signatures related to electrically aligned ice crystals are primarily caused by the differential propagation phase shift effects, to better eliminate the backscatter differential phase shift (δ) from the measured Φ_{DP} and obtain a reliable estimation of K_{DP} from smoothed Φ_{DP}, the finite impulse response (FIR) filter method (Hubbert & Bringi, 1995) is applied to smooth measured Φ_{DP} by using a large range window. Although a large window length could cause a loss of measured Φ_{DP} in the initial and final range gates along the radial paths, the absence of data in these regions will not impact the analysis of electrical alignment signatures in K_{DP}, due to measured Φ_{DP} is often affected by the influenced by ground clutter in near-range gates and a low signal-to-noise ratio in far-range bins. In this paper, employing the CSU_RadarTools package developed by a research group from Colorado State University (Lang et al., 2007), the unfolding measured Φ_{DP} is smoothed by using an FIR range filter with a window length of 4.5 km (60 range gates), and the measured Φ_{DP} with a standard deviation of differential phase $\sigma(\Phi_{DP})$ larger than 30° over 11 consecutive range gates is removed and replaced by linear interpolation of smoothed data. Then, the K_{DP} is estimated from the smoothed Φ_{DP} by using the least squares method, and calculated over a window whose length is inversely proportional to the corrected Z_H values, in which the rainfall attenuation is corrected by using the ZPHI method (Bringi et al., 2001; Park, Bringi, et al., 2005; Park, Maki, et al., 2005; Testud et al., 2000). Moreover, considering that the isolated thunderstorm is almost located within a distance of approximately 40 km of radar and the highest elevation angle is lower than 45°, the beam width of the MP-PAWR is less than 1.2° in azimuth direction and 1° in elevation direction, respectively. It suggests that the nonuniform beam-filling effect caused by the gradual broadening of the antenna beam along the distance was not significant, negative K_{DP} caused by a possible nonuniform beam-filling effect is neglected in this paper.

2.3. Methods to Study the Characteristics of Strong Electric Fields Related to the Upper Charge Regions in Thunderstorm

2.3.1. The Vertical Structure of the Average Electric Field Related to Upper Charge Regions Inferred by Vertical Profiles of the K_{DP}

The charge structure in thunderstorms is complex and characterized by multiple charge regions exhibiting alternating polarities. Taking the typical tripole charge structure as an example, the main negative charge region mainly consists of negatively charged graupel distributes at the midlevel of thunderstorms and normally sustains in a steady temperature level between −10 and −20°C, associated with moderate reflectivity (e.g., 30–45 dBZ), largely due to presence of graupel. The positively charged ice crystals are carried up to a high level to form the upper positive charge region, while the lower positive charge region with positively charged graupel is beneath the main negative charge region (Dye et al., 1986, 1988; Krehbiel, 1986; Saunders, 1993; Saunders et al., 2006; Williams, 1989, 2001). Considering that the main negative charge region maintains a relatively constant altitude range, the variations of electric fields in the upper parts of the thunderstorm are more likely associated with the electric charge accumulation and neutralization by lightning discharges in the upper charge regions.

In this paper, the negative K_{DP} signatures are employed to investigate the characteristics of electric fields associated with the upper charge regions. In the middle and the upper parts of thunderstorms, negative K_{DP} has been proven to be physically connected with the presence of electrically aligned ice particles with a mean orientation angle larger than 45°. It is important to note that the large graupel is too heavy to be aloft in the upper parts of thunderstorms, and the negative K_{DP} signature related to electrically aligned ice crystals normally cannot be masked by aggregates and small graupel (Carey et al., 2009; Hubbert, Ellis, Chang, Rutledge, & Dixon, 2014; Ryzhkov & Zrnić, 2007). Considering that, in this paper, the K_{DP} is estimated from the smoothed Φ_{DP} with a long-range window, and the decreased Φ_{DP} due to the depolarization effect associated with electrically aligned ice particles largely attributed to the cumulative propagation differential phase shift along the propagation path. This probably suggests that the influence of large hail on Φ_{DP} is normally smaller than the effect of electrically aligned ice particles, thus the impact on negative K_{DP} signatures of large hail could be neglected. Additionally, the negative K_{DP} value exhibits a linear increase (decrease) with increasing (decreasing) concentration of vertically aligned ice crystals and a non-linear connection with increasing (decreasing) particle sizes (Carey et al., 2009), while the increased concentration and/or size of electrically aligned vertically oriented ice crystals normally signifies the presence of more intense electric fields in the upper parts of thunderstorms. It suggests that, although the negative K_{DP} value in the range gate may be dominated by a few but large vertically aligned ice particles, such as plates with a large aspect ratio, a large amplitude of negative K_{DP} normally indicates the presence of a strong electric field in the vicinity of the gate. For example, an electric field of 100 kV/m can align plates smaller than 0.6 mm in diameter and columns larger than 2 mm. However, for larger plates, such as 1.7 mm plates, a field of 200 kV/m is required to align them (Caylor & Chandrasekar, 1996). Consequently, the electrical-related characteristics associated with the upper charge regions of the thunderstorm, including variations in strength and distribution of strong electric field, could be roughly qualitatively analyzed by the spatial distribution and variations in the negative K_{DP} within a selected region in the upper parts of thunderstorms.

To gain an intuitive understanding of the height-versus-time distribution of relative intensity of the strong electric fields related to the upper charge regions, we calculated the vertical profiles of K_{DP} by averaging the K_{DP} in a designated volume within the middle and upper parts of the isolated thunderstorm. Compared with limited elevations in the PPI scans of the conventional mechanical-scanning radar, the MP-PAWR can obtain vertical profiles from data observed within sufficient elevation angles in normal operation. Considering that the overall electric field structure in a thunderstorm changes at a slower rate compared to the rapid fluctuations in the local electric field responsible for individual lightning discharges, by taking advantage of the high spatio-temporal resolution of MP-PAWR, we utilize vertical profiles of the K_{DP} to investigate the distribution and variation in the degree of electrically aligned ice particles within the selected volume, which is associated with changes in the average electric field intensity and the spatial structure of the electric field related to the upper charge regions during the evolution of the isolated thunderstorm.

In this paper, the designated analysis volume responsible for the significant charging process of the isolated thunderstorm is selected by using composite reflectivity larger than 40 dBZ at and above an altitude of 7 km with an ambient temperature of about −10°C, and the gates with a correlation coefficient ρ_{HV} larger than 0.8 are retained. After interpolating the radar data in the selected volume from three-dimensional polar coordinates onto

three-dimensional Cartesian grids with the nearest-neighbor interpolation method, then in the cylindrical volume with irregular cross-section, the vertical profiles of K_{DP} are calculated by taking the layer-average of the K_{DP} value at each altitude range from an altitude of 7 km to the cloud top with the altitude resolution of 0.5 km. Considering that the isolated thunderstorm merged with other convective cells in the dissipation stage, only the radar data beyond 15 km from the radar are used to analyze, which means the highest elevation angle is lower than 45°. The K_{DP} was corrected for its dependency on the elevation angles based on Equation 1 which was theoretically derived from Baldini (Schneebeli et al., 2013). In this way, the K_{DP} values on higher elevations could be used for calculating the equivalent value of K_{DP} at 0° elevation.

$$K_{DP}(\theta = 0°) = K_{DP}(\theta \neq 0°)/\cos^2\theta \quad (1)$$

Where θ represents the elevation angle of 0°–45° in this paper.

2.3.2. Evaluation of IC Lightning Activity Potential by Using Composite K_{DP}

To evaluate the IC lightning activity potential of an isolated thunderstorm, we calculate the average composite K_{DP} in the analyzed volume and investigate the relationship between the average composite K_{DP} and IC lightning flash rate. The composite K_{DP} at a given layer corresponds to the minimum K_{DP} value observed in a vertical column across all elevation scans at each specific horizontal grid point at and above the designated layer (Wang et al., 2024). Given that the upper charge regions, distributed above the main charge region comprising charged graupel, predominantly consist of charged ice crystals, and the heightened negative K_{DP} signature typically corresponds to electrically aligned ice particles with large size or high concentration associated with intensified electric fields. Considering that ice particles gradually align vertically and exhibit negative K_{DP} signatures as a local strong electric field establishes and accumulates, and tend to reach a maximum alignment before IC lightning discharge, then rapidly recover to horizontal alignment due to the weakened electric field related to lightning discharges (Chandrasekar et al., 2023), the composite K_{DP} values at a given layer in the analyzed region could serve as a qualitative indicator of the strongest local electric field at and above the designated layer of the thunderstorm, which has the potential to trigger the IC lightning discharges. By calculating the average composite K_{DP} at a layer within the selected region, we can qualitatively evaluate the mean intensity of the strongest electric fields within the region. Then, the IC lightning activity potential in the region at and above the assigned layer of an isolated thunderstorm could be roughly evaluated. Furthermore, the relationship between IC lightning flash rate and the average composite K_{DP} at different layers in the analyzed region could be investigated.

In this paper, the analyzed volume contains the mixed-phased region which involves supercooled drops, riming particles, and ice crystals. Carey et al. (2009) investigated the alignment signatures of ice crystals in K_{DP} by modeling methods, and the results indicated that the negative K_{DP} signature of vertically oriented ice crystals is not affected by the horizontal arrangement of aggregates when they are mixed, and the same feature applies in a mixture of vertically aligned ice crystals and horizontally aligned graupel, with reflectivity ranging from 5 to 35 dBZ. For moderate to large reflectivity (40 to 45 dBZ), the presence of large graupel starts to influence the negative K_{DP} signature of vertically aligned ice crystals, particularly when reflectivity exceeds 45 dBZ. To improve the reliability of composite K_{DP} and avoid the effect of large graupel and hail, we calculated the composite K_{DP} at different altitudes within the range gate in which the Z_H is less than 45 dBZ, then calculated the average composite K_{DP} at the altitudes in the selected region, representing the mean value of maximum electric field intensity at and above corresponding altitudes in the analysis volume, meanwhile, the possible statistical errors of electrical alignment signature in negative K_{DP}, such as conical graupel, could be reduced.

2.3.3. Exploring the Correlation of IC Lighting Rate Associated With Negative K_{DP} Volume

Given that the total electric field changes over a longer time scale compared with fluctuation in local electric fields associated with lightning discharges, as a gradual intensification of the total electric field related to the upper charge regions with the evolution of a thunderstorm, it is reasonable to expect that a larger volume of ice particles will be affected by the strong electric field, exhibiting a large-area electrical alignment signature. Conversely, as the overall electric field weakens, this volume decreases. In this paper, the volume of negative K_{DP} is used to represent the volume of ice particles in the middle and upper parts of the isolated thunderstorm affected by the total electric field in-cloud associated with IC lightning discharges. The changes in negative K_{DP} volume are employed to qualitatively evaluate the variations in the strength of the total electric field within the upper parts of

the thunderstorm. In this paper, we employ the negative K_{DP} volume at and above an altitude of 7 km to explore its relationship with IC lightning flash rate in the isolated thunderstorm, and investigate the time-height evolution of the negative K_{DP} volume by calculating its vertical profile. To calculate the negative K_{DP} volume, the radar data on polar coordinates are interpolated onto a Cartesian coordinate with the nearest-neighbor interpolation method, with a height and a horizontal resolution of a grid cell volume are 0.5 and 0.1 km respectively. Subsequently, the negative K_{DP} volume is calculated by summing over all radar grid cells with the negative K_{DP} value at and above 7 km in the isolated thunderstorm, and then multiplying them by the grid cell volume. Moreover, considering the impact of noisy negative K_{DP} value near 0°/km, we also calculated the negative K_{DP} volume with the threshold of −0.25 and −0.5°/km, respectively, to compare the reliability of usage in negative K_{DP} volume. Besides, unless otherwise specified, the negative K_{DP} volume referred to in this paper is the volume calculated using negative K_{DP} with a threshold of 0°/km.

3. Observation Results and Analysis

3.1. Overview of the Isolated Thunderstorm

In this paper, we select an isolated thunderstorm that moved from the west to the southeast of the MP-PAWR on 20 August 2019, for analysis, as Figure 1 shows. In the following part of this paper, the Z_H and K_{DP} are the ones after the quality control process. Considering that the updraft intensity is related to the echo top height and the area of the echo with moderate reflectivity, we roughly defined the lifecycle of the isolated thunderstorm according to the echo top height and the 40 dBZ echo volume above an altitude of 7 km (Section 3.3.3) in the isolated thunderstorm. The developing stage of the isolated thunderstorm was from about 15:28:08 JST to 16:07:21 JST with a rapid increased cloud top height and 40 dBZ echo volume, while the mature stage was from about 16:07:21 JST to 16:27:39 JST with no significant decrease in cloud top height. After 16:27:39 JST, both the cloud top height and the 40 dBZ echo volume decreased rapidly, and the microphysical properties of the isolated thunderstorm during the dissipating stage are not analyzed because it merged with other convective cells. The first IC lightning flash in the isolated thunderstorm occurred at 15:40:03 JST in the early developing stage, and the IC lightning flash rate reached the peak of 88 flashes/min at 16:25:10 JST within the end of the mature stage. The Constant-Altitude Plan-Position Indicator (CAPPI) results at 10 km of the Z_H, K_{DP}, and ρ_{HV} at these two times are shown in the top and bottom panels of Figure 1, respectively. In the middle panel of Figure 1, at 16:07:21 JST, the CAPPI result of K_{DP} at 10 km exhibits a region of negative K_{DP} value with the ρ_{HV} larger than about 0.95, indicated of electrical alignment of ice particles related to strong electric fields. According to sounding data at the Tateno site on 20 August 2019, the ambient temperature at an altitude of 5.5 , 7, 8.5, 10, 11.2, and 12.5 km is about 0, −10, −20, −30, −40, and −50°C, respectively. Admittedly the environment sounding data could not fully represent the in-cloud temperature variabilities, so we use altitude as a rough proxy of isotherms.

3.2. The Electrical Alignment Signatures of Ice Crystals in the Isolate Thunderstorm

Figure 2 shows the time-height results of Z_H, K_{DP}, and ρ_{HV} in the isolated thunderstorm at a range of 27 km from the radar at a 249.6° azimuth, as shown by the triangular mark on the black line in Figure 1. The vertical cross-section results were obtained from radar data on three-dimensional Cartesian grids with an altitude resolution of 0.5 km. As Figure 2a shows, the echo top height ascended within the developing stage. During the mature stage, the reflectivity of the echo core was larger than 50 dBZ, and the height of the cloud top was eventually maintained at about 15 km. As Figure 2b shows, after 15:52:27 JST, a negative K_{DP} region emerged in the upper part of the isolated thunderstorm, around an altitude of about 10 km. After about 16:09:15 JST, this negative K_{DP} region expanded, reaching the top of the cloud. Significantly, there was a layer with an enhancement in the negative K_{DP} values observed between altitudes of 10 and 11 km, where the minimum K_{DP} value was smaller than −1°/km. The increasing amplitude and range in height of the negative K_{DP} region indicated intensified electric fields in the middle and upper parts of the thunderstorm, which is probably related to the enhanced upper charge regions with the increased concentration of the charged ice crystals. The ρ_{HV} values were generally greater than 0.95 in the negative K_{DP} region in the middle and upper part of the storm, as Figure 2c shows. Moreover, there was a region with K_{DP} values near zero, at an altitude of about 8.5 km, distributed between the negative K_{DP} and positive K_{DP} regions. According to the results from Biggerstaff et al. (2017), the main negative charge region is located along the bottom boundary of the negative K_{DP} region, exhibiting near zero to weakly positive K_{DP} values. Thus, it suggests this region with near zero K_{DP} was probably associated with the main negative charge region in the isolated thunderstorm.

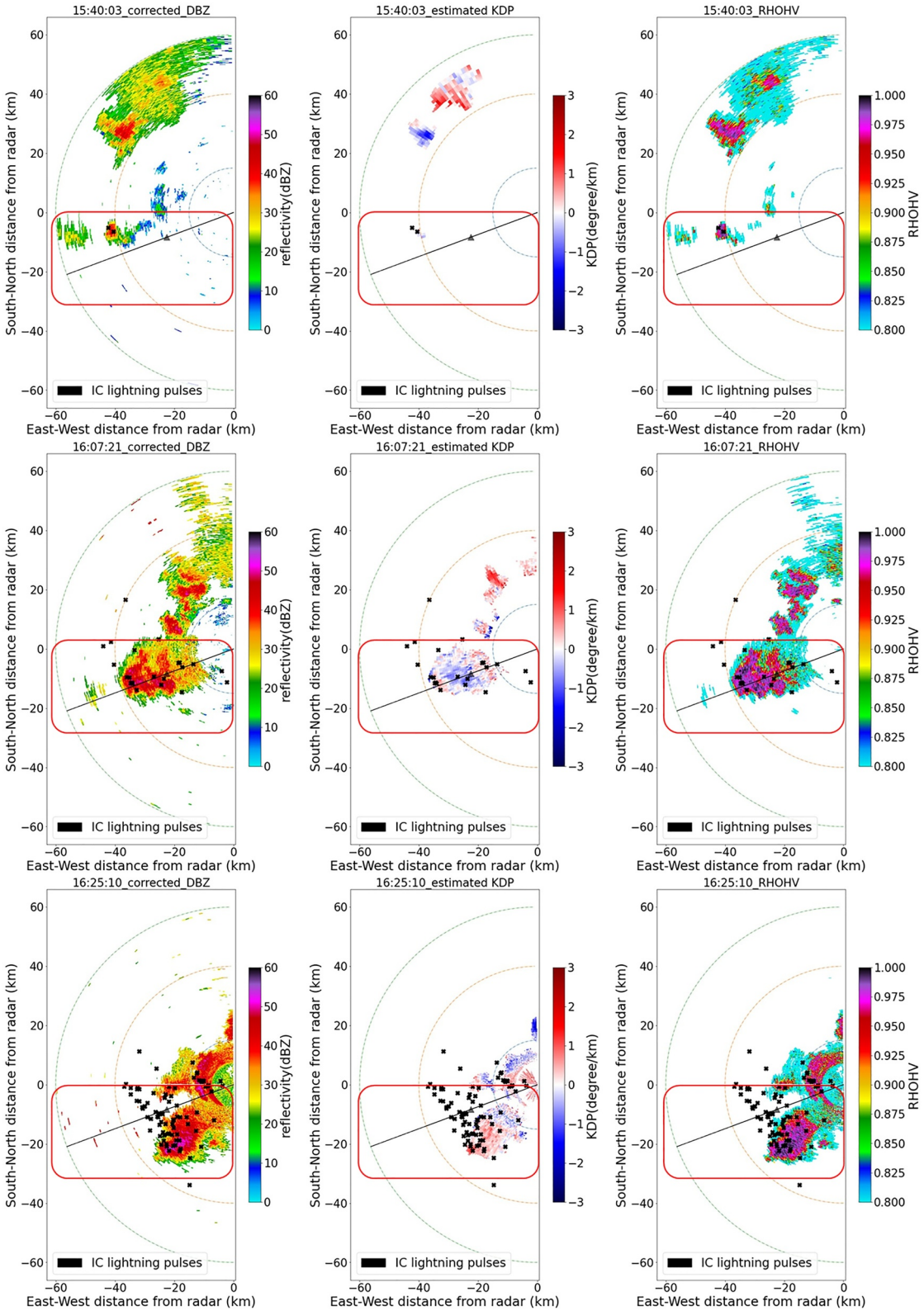

Figure 1.

Figure 3a shows the CAPPI results of the K_{DP} at 10 km at 16:09:15 JST. A negative K_{DP} region appeared at this height layer, with a minimum K_{DP} below −1°/km at an azimuth of 248.4°. Figures 3b–3d show the horizontal cross-section images of the composite K_{DP} at an altitude of 10 km at 16:09:15 JST, 16:09:45 JST, and 16:10:15 JST, respectively. Compared with the CAPPI of K_{DP}, Figure 3b shows a larger region with negative K_{DP} values, along with an increased negative K_{DP} area with K_{DP} less than −1°/km observed at the azimuth of 248.4°, as shown in Figure 3a. The lowest composite K_{DP} at 16:09:15 JST appeared at an azimuth of 258°, marked as black pixels in the red circle in Figure 3b, with a minimum K_{DP} below −2°/km. 30 seconds later, both of these negative K_{DP} regions at azimuths 248.4° and 258° shown in Figure 3b shrank as the nearby IC lightning pulses increased. At the same time, an intensified negative K_{DP} region appeared near the center marked by a red circle in Figure 3c, with a minimum value below −2°/km. Similarly, as shown in Figure 3d, the composite K_{DP} distribution at 16:10:15 JST illustrated that the negative K_{DP} region (marked with a red circle in Figure 3c) where the minimum K_{DP} was below −2°/km 30 s before has weakened, and the minimum value was above −1.5°/km, while the nearby IC lightning pulses increased. The result indicated that, compared with K_{DP}, the composite K_{DP} could exhibit a variation probably associated with IC lighting activity, with enhanced negative K_{DP} signature before IC lightning discharges and weakened after them. However, due to the lightning data being two-dimensional, further observations are required for this supposed result.

3.3. Characteristics of the In-Cloud Electric Fields Related to IC Lightning Flash Rate

In this paper, the analysis volume used to investigate the characteristics of strong electric fields related to the upper charge regions, as well as the correlation between negative K_{DP} signatures and IC lighting activity in the isolated thunderstorm, is determined by employing the presence of graupel signature, as described in Section 2.3.1. Only IC lightning discharges occurring within this designated volume, associated with the active non-inductive collisional charging region in the isolated thunderstorm, are used to calculate the IC lightning flash rate.

3.3.1. The Vertical Profiles of K_{DP} in the Middle and Upper Parts of the Isolated Thunderstorm and Their Relationship With IC Lightning Flash Rate

Figure 4 shows the time evolution of vertical profiles of K_{DP} in the isolated thunderstorm, calculated at each altitude within the selected volume on three-dimensional Cartesian grids, as described in Section 2.3.1. This result exhibits the vertical distribution and variation of the negative K_{DP} signature in the isolated thunderstorm, which could be used to explore the vertical structure of the average electric field in the middle and upper parts of the thunderstorm. In this paper, during the early developing stage of the thunderstorm, we analyzed the negative K_{DP} signatures at the cloud top using the results of the vertical profile of K_{DP} at and above 7 km. After the early developing stage, we focused primarily on the profile results above about 8.5 km. This is because, as the thunderstorm developed, the K_{DP} profile results in the lower part of the selected region are more likely to be influenced by large positive K_{DP} values of a large amount of supercooled drops rising with the updraft.

As Figure 4a shows, during the early developing stage, the negative K_{DP} initiated above 7 km and raised to 10 km with the updraft before 15:40:03 JST, which indicates ice particles gradually aligned by an electric field. It suggests that the electric field built up and accumulated in the upper parts of the isolated thunderstorm, associated probably with the accumulation of charged ice crystals lifted by the updrafts. The average K_{DP} value on the top of the cloud reached the minimum value that less than −1°/km at 30 s before the first IC lightning flash. The enhanced negative K_{DP} signature is caused by the stronger electric fields on the top of the cloud which probably caused the first IC lightning discharge. In the developing stage, there are two negative K_{DP} regions distributed in the middle and upper parts of the thunderstorm: a lower major negative K_{DP} region between 8.5 and 10 km, and a higher minor negative K_{DP} region on the top of the cloud. It probably indicates that these two regions, associated with strong electric fields, may correspond to the main upper positive charge region and a higher upper charge region.

Figure 1. Constant-Altitude Plan-Position Indicator (CAPPI) results at an altitude of 10 km of the isolated thunderstorm, on 20 August 2019. The top, middle, and bottom panel shows the results of attenuation corrected Z_H, estimated K_{DP}, and ρ_{HV} at 15:40:03 Japan Standard Time (JST), 16:07:21 JST, and 16:25:10 JST, respectively. The analyzed isolated thunderstorm located in a region as a red box marked. Three arcs represent 15, 40, and 60 km away from MP-PAWR. The black points are the intracloud (IC) lightning pulses. The black line is the azimuth angle of 249.6°, and a black triangle on the line represents the location 27 km away from the radar. The lightning pulses fall out of the CAPPI results at an altitude of 10 km because the data of lightning pulses is two-dimensional and distributed across all heights. The echo area in K_{DP} is smaller than that in Z_H due to the estimation algorithm of K_{DP}.

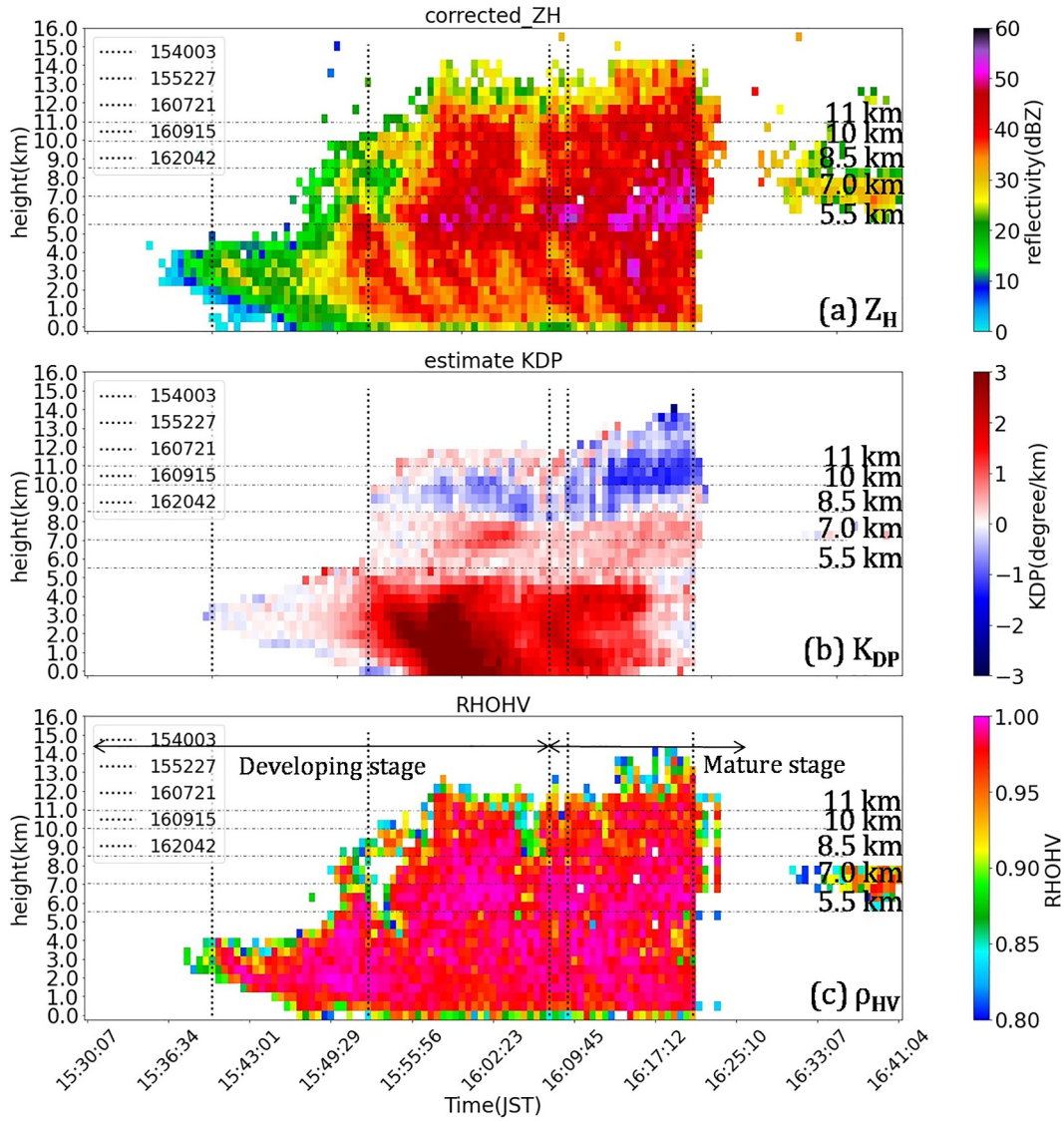

Figure 2. Time-height results of MP-PAWR at a range of 27 km from the radar at a 249.6° azimuth on 20 August 2019, Saitama University. (a): Z_H, (b): K_{DP}, (c): ρ_{HV}. The time resolution is 30 s and an altitude resolution is 500 m. The disappearance of the cloud echo after 16:20:42 Japan Standard Time was attributed to the movement of the thunderstorm.

During the mature stage of the isolated thunderstorm, until 16:20:42 JST, the negative K_{DP} regions raised and extended from the altitude of 10 km to the cloud top, with the greatest thickness distributed on the top of the thunderstorm shown as a red box in Figure 4a. It indicates extended electric fields in the upper parts of the cloud probably resulting from the increasing concentration of the upper charge regions, accompanied by possible intensified strong electric field on the top of the cloud represented by enhanced negative K_{DP} region with minimum values less than −1.5°/km. Meanwhile, the IC lightning rate gradually increased. It is noticed that, at the end of the mature stage, the IC lightning flash rate increased larger than 60 flashes/min and the maximum flash rate was 88 flashes/min. Concurrently, the negative K_{DP} region diminished, and most average K_{DP} values increased to positive values or near-zero positive values in the upper part of the thunderstorm. This suggests that in the middle and upper regions of the isolated thunderstorm, electric fields weakened during this period, likely due to the dissipation of upper charge regions caused by the large number of IC lightning discharges.

Figures 4b–4e show the vertical profiles of K_{DP} at different times during the developing stage and mature stage. Figure 4b shows the vertical profiles of K_{DP} from 15:35:35 JST to 15:39:33 JST in the early developing stage,

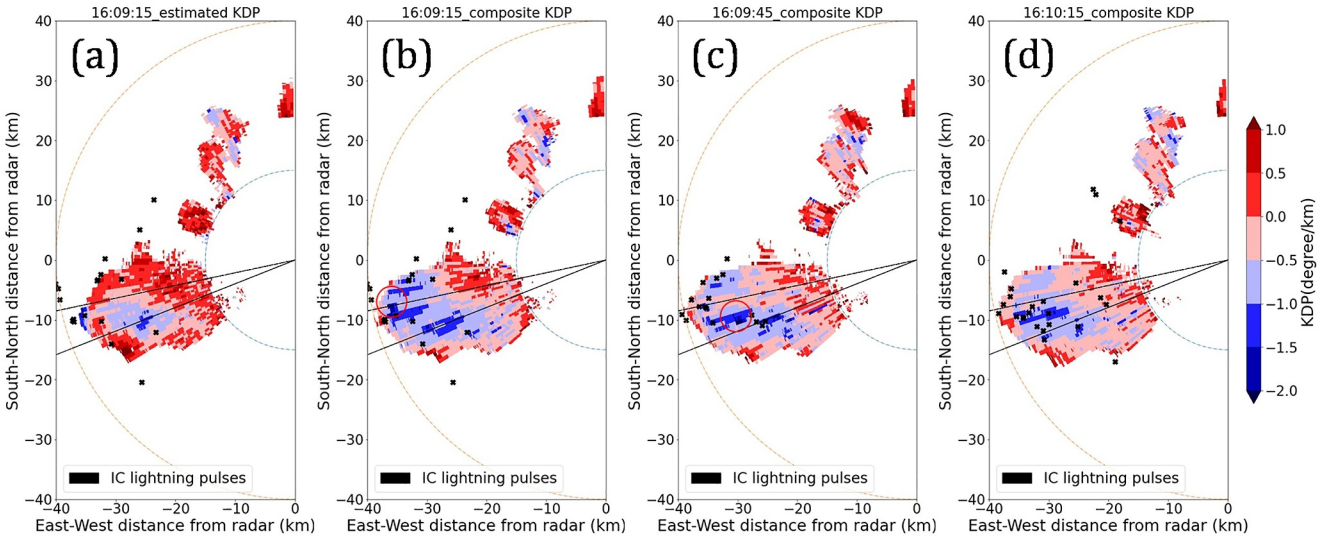

Figure 3. Horizontal cross-section results of K_{DP} and composite K_{DP} of the isolated thunderstorm at an altitude of 10 km, 20 August 2019, Saitama University. (a): K_{DP} at 16:09:15 Japan Standard Time (JST), (b)–(d): composite K_{DP} from 16:09:15 to 16:10:15 JST, time intervals are 30 s. Two arcs represent 15 and 40 km away from MP-PAWR. Two black lines represent the azimuths of 248.4° and 258°, respectively. The black crosses are the IC lightning pulses. The black pixels in the red circle in (b) and (c) mark points with the K_{DP} value less than −2°/km.

time intervals are 1 min. The vertical profiles of K_{DP} which started from 15:36:34 indicate strong electric fields related to the negative K_{DP} signature built up and accumulated above 7 km, and the top height of the electric fields raised accompanied by the decreased negative K_{DP} value. The vertical profile of K_{DP} at 15:39:33 JST (purple line in Figure 4b), 30 s before the first IC lighting flash, shows the intensified electric fields with a minimum K_{DP} value was almost −1.5°/km, and the top height of the vertical profile was above an altitude of 10 km. Figure 4c shows the vertical profiles of K_{DP} in the developing stage, the strong electric fields indicated by negative K_{DP} signature mainly distributed between 8.5 and 10 km. At 16:06:22 JST, shown as the purple line in Figure 4c, the average intensity and the height of the electric fields distributed below 10 km decreased compared with the result indicated by vertical profile at 4 min before (16:02:23 JST, red line in Figure 4c), and another strong electric field on the cloud top intensified above 12.5 km. These characteristics are consistent with the result shown as a black box in Figure 4a. In short, as the amplitude of negative K_{DP} values gradually increased, the center of the peak amplitude within the major negative K_{DP} regions gradually ascended, mainly distributed around 9 km (the ambient temperature is about −25°C) in the developing stage. This probably suggests that, with the progress of electrification, the electric fields ascended and primarily concentrated at an altitude of around 9 km within the isolated thunderstorm.

In the mature stage, shown in Figure 4d, the strong electric fields indicated by the negative K_{DP} distributed from 10 km to the cloud top. Compared to the vertical profile of K_{DP} at 16:06:22 JST (the purple line in Figure 4c), the vertical profile of K_{DP} between about 10 and 12.5 km changed from positive value to negative value at 16:07:21 JST (the black line in Figure 4d). The vertical profiles of K_{DP} above 10 km to the cloud top almost exhibited negative K_{DP} signature at 16:09:45 JST, 16:17:12 JST, and 16:20:10 JST, with the height of the most negative K_{DP} layer being higher than the height at 16:07:21 JST. It suggests that the electric field intensity increased and the intensity center shifted upwards, probably due to enhanced upper charge regions associated with the accumulative charged ice crystals by updrafts. Figure 4e shows the vertical profiles of K_{DP} at the end of the mature stage. At 16:20:42 JST, the K_{DP} value changed from negative to positive above 12.5 km (the black line in Figure 4e) which suggests that the electric fields above 12.5 km dissipated compared with the electric fields at 16:20:10 JST (the purple line in Figure 4d). Also, it is observed from the subsequent vertical profiles that the altitude with the peak amplitude of negative K_{DP} descended at 16:21:40 JST with decreasing amplitude. At 16:25:10 JST and 16:25:40 JST, there were only weak electric fields indicated by a slight negative K_{DP} signature above 11 km. It indicates that the strong electric fields related to the upper charge regions gradually weakened due to a large amount of lightning discharges.

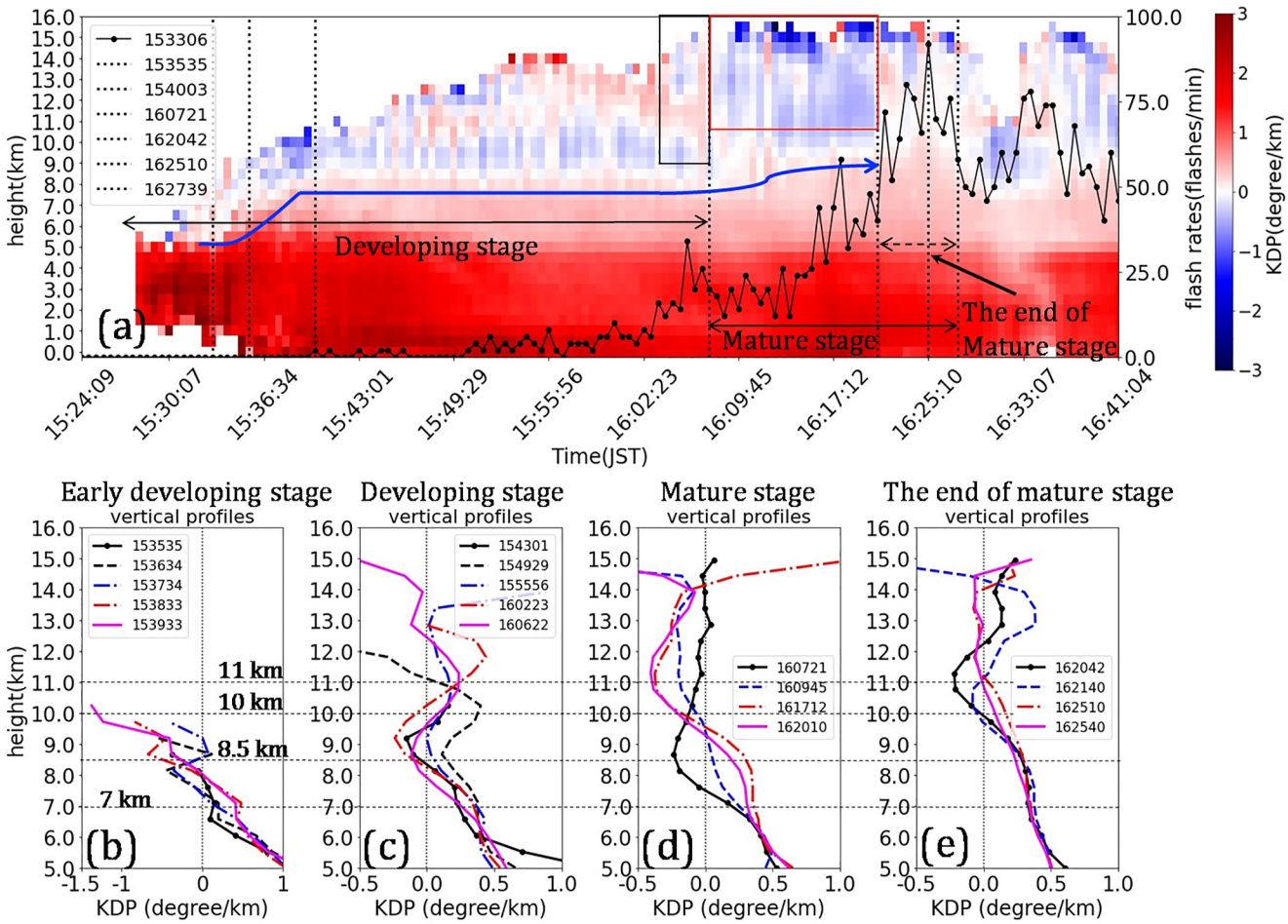

Figure 4. Vertical profiles of K_{DP} in the isolated thunderstorm. (a) Temporal evolution of vertical profiles of K_{DP}, (b)–(e) vertical profiles of K_{DP} from an altitude of 5 km to the cloud top at different times. In panel (a), the altitude range is from the ground to the cloud top and the altitude resolution is 0.5 km. The black line is the intracloud (IC) lightning flash rate, and the first IC lightning flash occurred at 15:40:03 Japan Standard Time which is marked as the third vertical dot line. The results of vertical profiles at altitude lower than 7 km are presented to better display the variation of K_{DP}.

Furthermore, there is a region, above a blue curve line marked in Figure 4a, distributed between the negative K_{DP} and bottom positive K_{DP} regions where the average K_{DP} values are near zero or slightly positive values. Similar to the result of the vertical cross-section in Figure 2, in the isolated thunderstorm, during the period before the end of the mature stage, the region probably indicated that the altitude of the main negative charge region probably ascended from about 7 to 8.5 km during the developing stage, then rose to about 9 km before the end of the mature stage. However, it should be noted that the main negative charge region is inferred by comparing the average K_{DP} results with the vertical cross-section results of K_{DP} on more locations in the thunderstorm (one of them is shown as Figure 2b), rather than just inferring from the average K_{DP} results. It is because the average K_{DP} results, especially at lower altitudes, such as the near-zero average K_{DP} around 8 km, are susceptible to be affected by hydrometeors with large positive K_{DP}, such as a large amount of supercooled drops.

In sum, based on the temporal evolution of the vertical profiles of K_{DP} throughout the isolated thunderstorm's lifecycle, the height of radar-inferred strong electric fields related to the upper charge regions gradually raised from the early development stage until the end of the mature stage, while the altitude of the maximum intensity of the electric fields elevated and sustained at about 11 km before the end of the mature stage with gradual intensification. Meanwhile, the altitude of the possible main negative charge region ascended from about 7 to 9 km, and during most of the development stage, it was distributed at an altitude of about 8.5 km. During this period, the IC lightning rate gradually increased. Subsequently, the height of the strong electric fields related to the upper charge

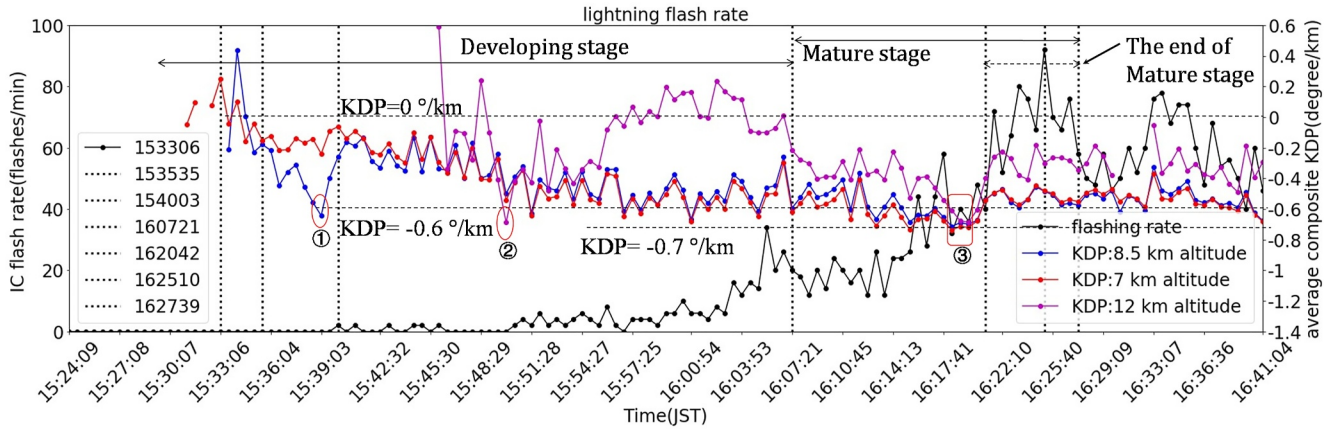

Figure 5. Time series of the intracloud (IC) lightning flash rate and the averaged composite K_{DP} of the isolated thunderstorm. The black line is the IC lightning flash rate. The first IC lightning flash occurred at 15:40:03 Japan Standard Time (JST) (marked as the third vertical black line). The blue line, red line, and purple line represent the average composite K_{DP} values at altitudes of 7, 8.5, and 12 km, respectively. The three horizontal black dashed lines from top to bottom represent K_{DP} values equal to 0, −0.6, and −0.7°/km, respectively. The red circle with the number 1 indicates that the average composite K_{DP} at 8.5 km reached its minimum value 1 min before the first IC lightning flash, while the red circle with the number 2 indicates that the average composite K_{DP} at 12 km reached its minimum value at 15:49:58 JST, which may be related to subsequent IC lightning discharges. The red box marked as number 3 represents that the average composite K_{DP} at the three altitudes reached the minimum values at about 5.5 min before the peak of IC lightning rate.

regions descended with the weakening of the electric field, while the IC lightning rate increased and reached its maximum and then declined.

3.3.2. Relationship Between Composite K_{DP} and IC Lightning Flash Rate

Figure 5 shows the time evolution of the IC lightning flash rate and the average composite K_{DP} values at altitudes of 7, 8.5, and 12 km in the selected volume of the isolated thunderstorm, which are calculated within radar gates in which the Z_H is less than 45 dBZ at and above a designated altitude in the selected volume. Besides, the selected volume used to calculate composite K_{DP} is the same region selected by using the method indicated in Section 2.3.1, but without projecting onto three-dimensional Cartesian grids due to resolution considerations.

In the early developing stage, 1 min before the first IC lighting flash, the average composite K_{DP} at 7 and 8.5 km decreased from positive values to negative values and reached minimum negative values. The average composite K_{DP} at 8.5 km gradually decreased from the maximum positive value of 0.4°/km to a minimum negative value of less than −0.6°/km in 5 min (from 15:34:10 JST to 15:39:03 JST), subsequently increased to about −0.1°/km following the IC lightning discharges. It probably indicates a gradual strengthening of electric fields at and above 8.5 km, reaching their peak approximately 1 min before the first lightning flash, followed by a subsequent weakening due to lightning discharges. Similar features again appeared at 12 km from 15:49:29 JST to 15:49:58 JST, the averaged composite K_{DP} value decreased from about 0.2°/km to a minimum value of less than −0.6°/km and subsequently increased following the IC lightning discharges. After the first IC lightning flash at 15:40:03 JST, the averaged composite K_{DP} at 7 and 8.5 km gradually decreased as the IC lighting flash rate increased, indicative of intensified electric fields above 8.5 km. It is noticed that, before 16:07:21 JST, the average composite K_{DP} at 12 km exhibits positive K_{DP} values compared with the average composite K_{DP} at 7 and 8.5 km. It indicates that strong electric fields related to the upper charge regions mainly distributed between 8.5 and 12 km before 16:07:21 JST.

During the mature stage of the isolated thunderstorm before 16:20:42 JST, the average composite K_{DP} at 7 km, 8.5 km, and 12 km decreased as an increasing IC lightning flash rate, reached minimum negative values about −0.7°/km at about 16:19:41 JST 5.5 min before peak of IC lightning rate. Meanwhile, the average composite K_{DP} at 12 km dropped greater than the values at lower altitudes, indicating that the strong electric fields appeared above 12 km and gradually intensified. Besides, the amplitude of the average composite K_{DP} at 12 km was smaller than the values at lower altitudes, indicating that the maximum strength of electric fields mainly concentrated below 12 km. At the end of the mature stage, from 16:20:42 to 16:27:39, the IC lightning rate increased to the peak and then decreased, while the average composite K_{DP} values at the three altitudes both increased. It probably

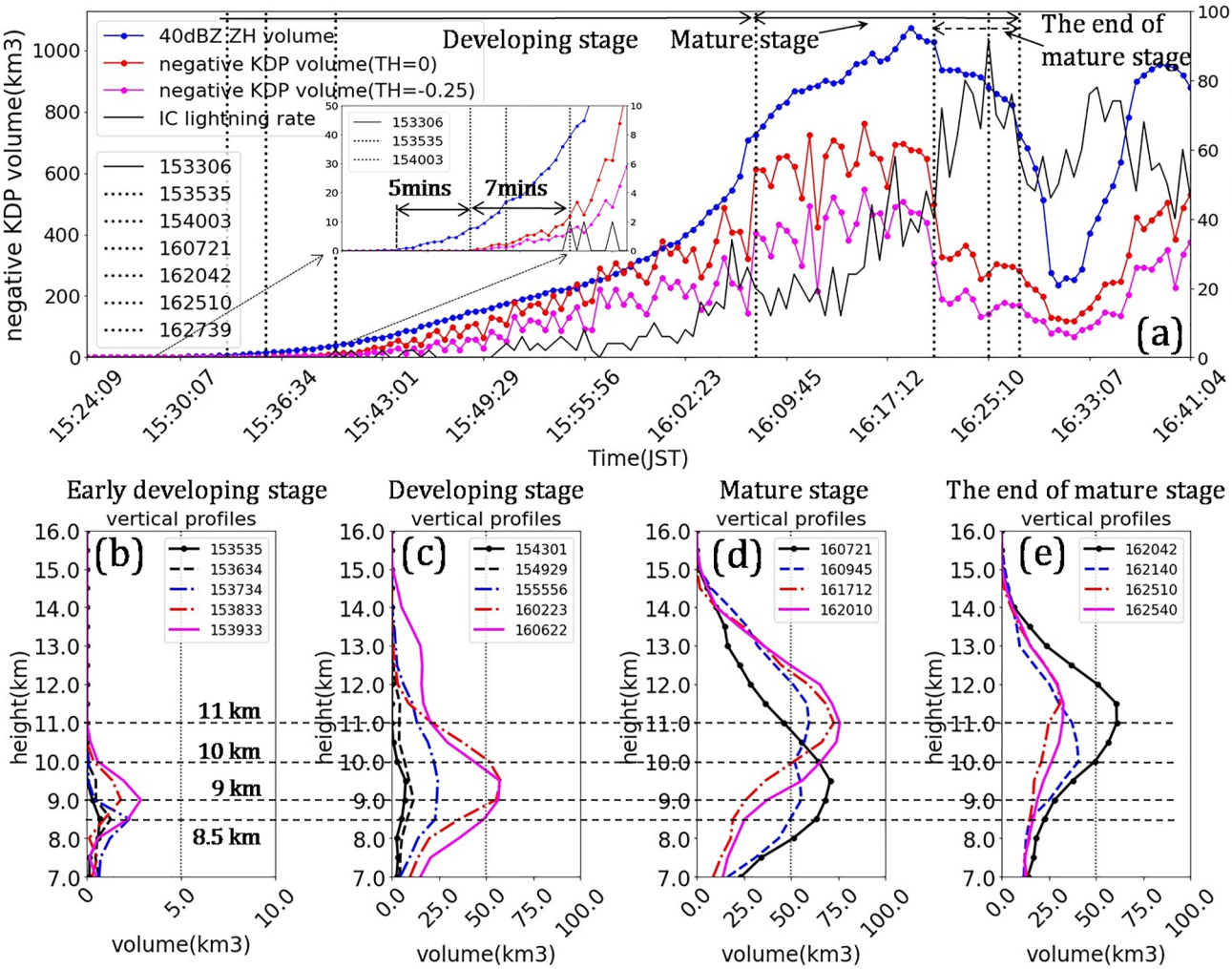

Figure 6. (a) Time series of negative K_{DP} volume (km^3), 40 dBZ echo volume (km^3), and intracloud (IC) lightning flash rate. The red line is the negative K_{DP} volume (threshold = 0°/km), the magenta line is the negative K_{DP} volume (threshold = −0.25°/km), the blue line is the 40 dBZ echo volume, the black line is the IC lighting flash rate; (b)–(e) vertical profiles of negative K_{DP} volume (threshold = 0°/km) at different stages.

means that the strong electric fields in the middle and upper parts of the thunderstorm weakened due to the large number of IC lightning discharges.

The variation in average composite K_{DP} values at different altitudes roughly depicted the evolution of the strongest local electric field within the middle and upper parts of the isolated thunderstorm, which is nearly consistent with the change in electric field inferred by using vertical profiles of K_{DP} in Section 3.3.1. Furthermore, the signature that the average composite K_{DP} at an altitude gradually decreases from a positive value to a negative value, or becomes more negative, signifies a progressively strengthening electric field. This intensifying field probably leads to increased IC lightning activity above the altitude in isolated thunderstorms. In addition, there is a tendency for the IC lightning rate to increase as the average composite K_{DP} decreases in the middle and upper layers of the thunderstorm. The peak IC lightning rate lagged behind the minimum average composite K_{DP} by approximately 5.5 min.

3.3.3. Relationship Between Negative K_{DP} Volume and IC Lightning Flash Rate

Figure 6a shows the time evolution of the negative K_{DP} volume and the IC lightning flash rate. In the developing stage, the negative K_{DP} volume above 7 km increased to over about 600 km^3 as the IC lightning flash rate increased, and the peak IC lighting flash rate in the developing stage was less than 40 flashes/minute. During the mature stage before 16:20:42 JST, the negative K_{DP} volume increased slowly and varied between 600 and

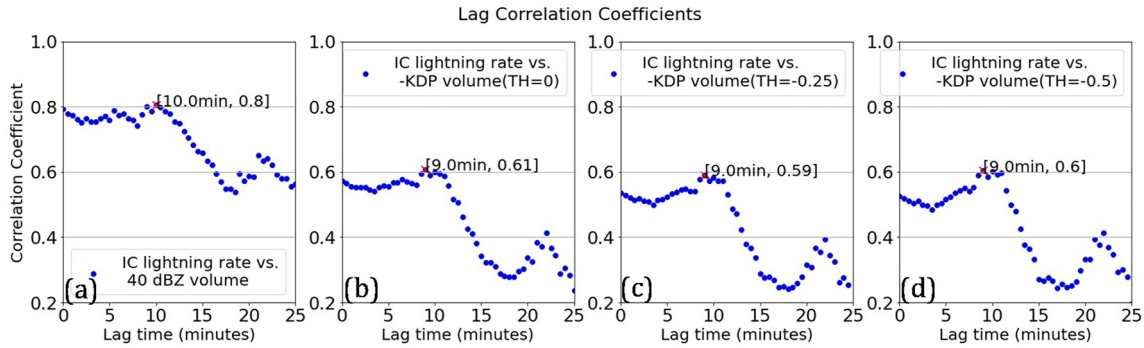

Figure 7. Time lagged correlation coefficients: (a) between intracloud (IC) lightning rate and 40 dBZ volume, (b)–(d) between IC lightning rate and negative K_{DP} volume calculated with different thresholds of 0, −0.25, and −0.5°/km, respectively.

700 km^3, the peak value of the negative K_{DP} volume was about 720 km^3 and about 9.5 min before the peak value of the IC lightning flash rate. During the end of the mature stage, the negative K_{DP} volume decreased approximately from 650 km^3 to about 500 km^3 at 16:20:42 JST, then continued to gradually decrease to about 300 km^3, while the IC lightning flash rate reached the peak at 16:25:10 JST and then decreased.

Figures 6b–6e show the temporal evolution of vertical profiles of negative K_{DP} volume. Figure 6b illustrates a gradual increase in the negative K_{DP} volume during the early developing stage, extending vertically with the updrafts, peaking at about 3 km^3 at an altitude of 9 km, just 30 s before the first IC lightning flash. Starting from the developing stage until the time before the end of the mature stage (as shown in Figures 6c and 6d), both the vertical extent and the negative K_{DP} volume increased, and the altitude of the maximum negative K_{DP} volume ascended. Meanwhile, the IC lightning rate continues to increase. It probably suggests that the total electric field intensified in the middle and upper parts of the thunderstorm, accompanied by a rise in the center of the strong electric field. Particularly, after 15:49:29 JST (the black dot line in Figure 6c), there was a rapid increase in both the total and maximum negative K_{DP} volume. The strong electric field represented by the negative K_{DP} volume mainly distributed between 8.5 and 10 km in the developing stage (shown in Figure 6c) with the center of the maximum negative K_{DP} volume of about 9 km, while it primarily centered around 11 km in the mature stage (shown in Figure 6d). During the end of the mature stage (shown in Figure 6e), the negative K_{DP} volume decreased, especially after 16:20:42 JST (the black line in Figure 6e), which probably indicated the electric fields weakened due to a large number of lightning discharges. In short, the variation and distribution of the total electric field inferred by negative K_{DP} volume is consistent with the result inferred from vertical profiles of K_{DP}, shown in Figure 4.

To investigate the relationship between the negative K_{DP} volume and IC lightning flash rate, we utilize the 40 dBZ echo volume in the upper parts of the thunderstorm for comparison. The 40 dBZ echo volume is calculated by summing the volume cells where the horizontal reflectivity Z_H at and above 7 km was greater than 40 dBZ in Cartesian coordinate grids, shown as the blue line in Figure 6. Besides, to evaluate the reliability of the negative K_{DP} volume, we calculated and compared the negative K_{DP} volumes with thresholds of −0.25 and −0.5°/km, respectively. Since these volumes show similar variation trends to the negative K_{DP} volume with a 0°/km threshold, we primarily analyze the results for the negative K_{DP} volume with the 0°/km threshold. For clarity, the negative K_{DP} volume with the −0.5°/km threshold is not shown in Figure 6a, but its correlation results are presented in Figure 7. As indicated in the small window of Figure 6, during the early developing stage, if we take the appearance of the 40 dBZ echo volume as the indicator of graupel formation, the time delay was about 12 min between the formation of graupel and the first IC lightning flash, and the formation of graupel occurred about 5 min earlier than the appearance of the strong electric fields represented by negative K_{DP} volume in the early developing stage. It was probably caused by the effect that large graupel has the potential to mask the negative K_{DP} signatures of electrically aligned ice crystals when they are mixed up within the electrification initiation stage, and the time is required for the charge layers to develop via differential gravitational sedimentation and the action of the updraft on the graupel and ice crystals. During the mature stage, a more stable variation in the 40 dBZ echo volume was observed compared to the variation in the negative K_{DP} volume. Especially at the end of the mature stage, the decrease in negative K_{DP} volume was more severe than the decrease in the 40 dBZ echo volume,

which probably suggests that a weakening electric field caused by a large number of lightning discharges, while the variations of the 40 dBZ echo volume are not as significant. This is probably because, in the middle and upper parts of a thunderstorm, the electrical alignment signature in negative K_{DP} is closely related to the intensity of the electric field.

As the results suggest, the intensified total electric fields, indicated by increasing negative K_{DP} volume above 7 km of the isolated thunderstorm, corresponded with increased IC lightning activity, while a large amount of IC lightning discharges during the end of the mature stage led to the strong electric fields collapse represented by a decline in negative K_{DP} volume, subsequently followed by decreased IC lightning activity. The IC lightning flash rate correlated and tended to lag with the evolution of the radar-inferred electric fields, with a correlation coefficient of 0.61 at a time lag of about 9 min, as Figure 7b shows. Besides, the IC lighting flash rate and the 40 dBZ volume have a strong correlation with the coefficient of 0.8 at a lag of 10 min (shown in Figure 7a), while the negative K_{DP} volumes calculated with different thresholds showed correlations of about 0.6 with the IC lightning flash rate at the same lag of 9 min (shown in Figures 7c and 7d).

4. Summary and Discussion

Considering that small ice particles in the upper part of a thunderstorm can be electrically aligned by a strong electric field, these particles gradually orient vertically with the build-up and accumulation of the strong electric field. Once the strong electric field dissipates, the ice particles recover to aerodynamic alignment within a time scale on the order of 10 milliseconds. Typically, the accumulation of the local electric field between lightning discharges causes the degree of electrical alignment of the ice particles to enhance continuously for several seconds or a time scale on the order of 10 s (Chandrasekar et al., 2023). The MP-PAWR, running in its operational mode with its high temporal resolution of 30 s, enables it to observe the electrical alignment signatures in the negative K_{DP} associated with local electric field variations related to lightning discharges. Moreover, in terms of the electrification process of thunderstorms, the variation in the total electric field occurs over a longer period. This suggests that, by employing the negative K_{DP} signatures, the MP-PAWR has the potential to perform instantaneous observation of the radar-inferred electric field in the electrification process within the evolution of thunderstorms.

In this paper, the negative K_{DP} signatures, investigated by vertical profiles of K_{DP}, composite K_{DP}, and negative K_{DP} volume, are employed to explore the characteristics of the radar-inferred electric fields associated with the upper charge regions in an observation of an isolated thunderstorm. The results show that the temporal progression of the vertical profiles of K_{DP} could be used to qualitatively examine the evolution in the vertical structure of the average electric field in the middle and upper parts of the isolated thunderstorm, including the height distribution and the variation of relative intensity. Meanwhile, based on the variation of the vertical profiles of K_{DP}, average composite K_{DP}, and the negative K_{DP} volume, the evolution of the radar-inferred electric fields corresponded with the electrification process of the isolated thunderstorm, including the initiation, intensification, and decay, and was well-depicted by variations in the IC lightning flash rate. Furthermore, the negative K_{DP} volume above an altitude of 7 km in the isolated thunderstorm, which is used for the first time to explore the relationship with lightning flash rate, exhibits a well correlation with IC lightning flash rate.

In this paper, the result of vertical profiles of K_{DP}, in a selected volume within the middle and upper parts of the isolated thunderstorm, exhibits a strong electric field mainly distributed between about 8.5 and 10 km during the developing stage, built up above an altitude of about 7 km at least 7 min before the first IC lightning flash in the early developing stage. In the mature stage, the radar-inferred strong electric field mainly distributed from 10 km to the cloud top with the strongest electric field concentrated around about 11 km with increasing intensity, as well as increasing IC lightning flash rate. During the end of the mature stage, the IC lightning flash rate kept a gradual increase and reached a peak, followed by a decline. Meanwhile, the electric field weakened probably due to the large number of lightning discharges.

Furthermore, in the isolated thunderstorm, we employed the composite K_{DP} to investigate the variation associated with the strongest local electric field above a designated altitude and the negative K_{DP} volume to explore the evolution in the total electric field. Thereby, the average composite K_{DP} could serve as an indicator of IC lightning activity potential above the altitude, while the negative K_{DP} volume is used to evaluate the correlation of total electric field intensity with IC lightning activity. In this paper, we explore the relationship between the average composite K_{DP} at different altitudes from 7 to 12 km, and the negative K_{DP} volume above 7 km with the IC

lightning flash rate in the selected volume of the thunderstorm. The results of vertical distribution and evolution radar-inferred electric field structure by employing average composite K_{DP} and negative K_{DP} volume are nearly consistent with the result of vertical profiles of K_{DP}. Compared with the negative K_{DP} volume, the average composite K_{DP} at 8.5 and 12 km revealed that the strong electric fields on the top of the cloud reached the maximum at 15:39:03 JST and 15:49:58 JST, respectively, as well as the weakened electric fields probably caused by subsequent lightning discharges. During the end of the mature stage, the average composite K_{DP} at 7 km, 8.5 km, and 12 km reached the minimum values about 7 min before the peak of the IC lightning flash rate, while the maximum negative K_{DP} volume appeared about 9.5 min before it.

Although the observation results in this paper demonstrate that the evolution of the radar-inferred electric fields in the middle and upper parts of the isolated thunderstorm corresponded well with the IC lightning flash rate, and the preliminary conclusions validate the potential use of negative K_{DP} signatures for lightning activity research, further research is needed to verify and improve the reliability of the conclusions. First, since the results in this paper are based on only an isolated thunderstorm case. In this case, the analysis volume is selected by using a reflectivity-based method indicating graupel presence. This approach ensures that the analysis region associated with the mixed-phase region, which plays a crucial role in the electrification process according to the non-inductive charging theory, is under examination. It should be noted that the vertical profiles used in this paper calculate the average K_{DP} value from all particles in the analysis volume containing the mixed-phase region. This indicates that the results at lower heights in the vertical profile could be influenced by hydrometeors with large positive K_{DP} value located in the lower parts of the analysis volume, such as supercooled droplets distributed primarily in the temperature range of 0 to −20°C. This implies that, especially in low-altitude areas of the mixed-phase region, further research on the characteristics of electrically aligned ice particles should be conducted by combining other polarimetric parameters. On this basis, the radar-inferred main negative charge region in this paper, which is distributed at around 8.5 km between positive and negative K_{DP} regions, could be more reliable, thereby improving the accuracy of the vertical profile results. Second, the real electric field structure in thunderstorms is complex, associated with different charge structures inside and outside the strong updrafts (Stolzenburg, Rust, Smull, & Marshall, 1998; Stolzenburg, Rust, & Marshall, 1998). In this paper, the electrically aligned ice crystals located outside the defined analysis volume are not taken into account, such as those in the anvil of the thunderstorm. Moreover, the negative K_{DP} value of electrically oriented ice crystals is affected by several factors, including the mean canting angle, particle size, concentration, and the intensity of the electric field within their vicinity. These issues have brought uncertainty to investigate the relationship between negative K_{DP} signatures and IC lightning flash rate, requiring more case studies and further analysis and validation combined with microphysics and kinematic structure of thunderstorms, and specific observation data of lightning, such as three-dimensional lightning location data. Additionally, this paper only employed two-dimensional lightning data to evaluate the correlation between negative K_{DP} signatures of electrically aligned ice particles in the upper part of the thunderstorm, the characteristics of the radar-inferred strong electric field, and the IC lightning rate. It is necessary to use three-dimensional lightning data in future studies to conduct further analysis of more thunderstorm cases. In future research, it will be necessary to use three-dimensional lightning data for observation and analysis in more cases. Only in this way can the electric alignment signatures of ice particles be fully utilized, combined with other methods such as echo volume, graupel volume, etc., to provide more accurate and in-depth observation and research on the evolution of strong electric fields in the upper regions throughout the thunderstorm lifecycle, as well as the relationship with IC lightning flash rate.

Data Availability Statement

The Environmental sounding data are available on the website of the University of Wyoming, https://weather.uwyo.edu/upperair/sounding.html. The LIDEN data and the MP-PAWR radar data on 20 August 2019, which was provided by NICT used in this paper are available in Wang (2023a, 2023b). The K_{DP} estimation algorithm is available in CSU_RadarTools version 1.3 (Timothy et al., 2019).

Acknowledgments
This study was supported by JSPS KAKENHI Grants 21H015920 and 24H00272. The operation of the Saitama MP-PAWR was supported by Cross-ministerial Strategic Innovation Promotion Program (SIP) of the Cabinet Office. Data of the Saitama MP-PAWR is provided by National Institute of Information and Communications Technology (NICT).

References

Baker, M. B., Blyth, A. M., Christian, H. J., Latham, J., Miller, K. A., & Gadian, A. M. (1999). Relationships between lightning activity and various thundercloud parameters: Satellite and modelling studies. *Atmospheric Research*, *51*(3–4), 221–236. https://doi.org/10.1016/S0169-8095(99)00009-5

Baker, M. B., Christian, H. J., & Latham, J. (1995). A computational study of the relationships linking lightning frequency and other thundercloud parameters. *Quarterly Journal of the Royal Meteorological Society*, *121*(527), 1525–1548. https://doi.org/10.1002/qj.49712152703

Basarab, B. M., Rutledge, S. A., & Fuchs, B. R. (2015). An improved lightning flash rate parameterization developed from Colorado DC3 thunderstorm data for use in cloud-resolving chemical transport models. *Journal of Geophysical Research: Atmospheres*, *120*(18), 9481–9499. https://doi.org/10.1002/2015JD023470

Biggerstaff, M. I., Zounes, Z., Addison Alford, A., Carrie, G. D., Pilkey, J. T., Uman, M. A., & Jordan, D. M. (2017). Flash propagation and inferred charge structure relative to radar-observed ice alignment signatures in a small Florida mesoscale convective system. *Geophysical Research Letters*, *44*(15), 8027–8036. https://doi.org/10.1002/2017GL074610

Bringi, V. N., Keenan, T. D., & Chandrasekar, V. (2001). Correcting C-band radar reflectivity and differential reflectivity data for rain attenuation: A self-consistent method with constraints. *IEEE Transactions on Geoscience and Remote Sensing*, *39*(9), 1906–1915. https://doi.org/10.1109/36.951081

Calhoun, K. M., MacGorman, D. R., Ziegler, C. L., & Biggerstaff, M. I. (2013). Evolution of lightning activity and storm charge relative to dual-Doppler analysis of a high-precipitation supercell storm. *Monthly Weather Review*, *141*(7), 2199–2223. https://doi.org/10.1175/MWR-D-12-00258.1

Carey, L. D., Petersen, W. A., & Deierling, W. (2009). Radar differential phase signatures of ice orientation for the prediction of lightning initiation and cessation. In *34th conference on radar meteorology (No. M09-0584)*.

Carey, L. D., & Rutledge, S. A. (1996). A multiparameter radar case study of the microphysical and kinematic evolution of a lightning producing storm. *Meteorology and Atmospheric Physics*, *59*(1–2), 33–64. https://doi.org/10.1007/bf01032000

Carey, L. D., & Rutledge, S. A. (1998). Electrical and multiparameter radar observations of a severe hailstorm. *Journal of Geophysical Research*, *103*(D12), 13979–14000. https://doi.org/10.1029/97JD02626

Carey, L. D., & Rutledge, S. A. (2000). The relationship between precipitation and lightning in tropical island convection: A C-band polarimetric radar study. *Monthly Weather Review*, *128*(8), 2687–2710. https://doi.org/10.1175/1520-0493(2000)128%3C2687:TRBPAL%3E2.0.CO;2

Carey, L. D., Schultz, E. V., Schultz, C. J., Deierling, W., Petersen, W. A., Bain, A. L., & Pickering, K. E. (2019). An evaluation of relationships between radar-inferred kinematic and microphysical parameters and lightning flash rates in Alabama storms. *Atmosphere*, *10*(12), 796. https://doi.org/10.3390/atmos10120796

Caylor, I., & Chandrasekar, V. (1996). Time-varying ice crystal orientation in thunderstorms observed with multiparameter radar. *IEEE Transactions on Geoscience and Remote Sensing*, *34*(4), 847–858. https://doi.org/10.1109/36.508402

Chandrasekar, V., Beauchamp, R. M., & Bechini, R. (2023). *Introduction to dual polarization weather radar*. Cambridge University Press.

Cho, H. R., Iribarne, J. V., & Richards, W. G. (1981). On the orientation of ice crystals in a cumulonimbus cloud. *Journal of the Atmospheric Sciences*, *38*(5), 1111–1114. https://doi.org/10.1175/1520-0469(1981)038<1111:OTOOIC>2.0.CO;2

Deierling, W., Latham, J., Petersen, W. A., Ellis, S. M., & Christian Jr, H. J. (2005). On the relationship of thunderstorm ice hydrometeor characteristics and total lightning measurements. *Atmospheric Research*, *76*(1–4), 114–126. https://doi.org/10.1016/j.atmosres.2004.11.023

Deierling, W., & Petersen, W. A. (2008). Total lightning activity as an indicator of updraft characteristics. *Journal of Geophysical Research*, *113*(D16), D16210. https://doi.org/10.1029/2007JD009598

Deierling, W., Petersen, W. A., Latham, J., Ellis, S., & Christian, H. J. (2008). The relationship between lightning activity and ice fluxes in thunderstorms. *Journal of Geophysical Research*, *113*(D15), 306. https://doi.org/10.1029/2007JD009700

Deierling, W., Petersen, W. A., Latham, J., Ellis, S. M., Christian, H., & Walters, J. T. (2006). Total lightning frequency in relation to ice masses and ice mass flux estimates. In *Preprints, second conference on meteorological applications of lightning data, Atlanta, GA, American Meteorological Society P* (Vol. 2).

Dolan, B., Rutledge, S. A., Lim, S., Chandrasekar, V., & Thurai, M. (2013). A robust C-band hydrometeor identification algorithm and application to a long-term polarimetric radar dataset. *Journal of Applied Meteorology and Climatology*, *52*(9), 2162–2186. https://doi.org/10.1175/JAMC-D-12-0275.1

Dye, J. E., Jones, J. J., Weinheimer, A. J., & Winn, W. P. (1988). Observations within two regions of charge during initial thunderstorm electrification. *Quarterly Journal of the Royal Meteorological Society*, *114*(483), 1271–1290. https://doi.org/10.1002/qj.49711448306

Dye, J. E., Jones, J. J., Winn, W. P., Cerni, T. A., Gardiner, B., Lamb, D., et al. (1986). Early electrification and precipitation development in a small, isolated Montana cumulonimbus. *Journal of Geophysical Research*, *91*(D1), 1231–1247. https://doi.org/10.1029/JD091iD01p01231

Dye, J. E., Winn, W. P., Jones, J. J., & Breed, D. W. (1989). The electrification of New Mexico thunderstorms: 1. Relationship between precipitation development and the onset of electrification. *Journal of Geophysical Research*, *94*(D6), 8643–8656. https://doi.org/10.1029/JD094iD06p08643

Fehr, T., Dotzek, N., & Höller, H. (2005). Comparison of lightning activity and radar-retrieved microphysical properties in EULINOX storms. *Atmospheric Research*, *76*(1–4), 167–189. https://doi.org/10.1016/j.atmosres.2004.11.027

Foster, T. C., & Hallett, J. (2002). The alignment of ice crystals in changing electric fields. *Atmospheric Research*, *62*(1–2), 149–169. https://doi.org/10.1016/S0169-8095(02)00008-X

Foster, T. C., & Hallett, J. (2008). Enhanced alignment of plate ice crystals in a non-uniform electric field. *Atmospheric Research*, *90*(1), 41–53. https://doi.org/10.1016/j.atmosres.2008.02.017

Goodman, S. J., Buechler, D. E., Wright, P. D., & Rust, W. D. (1988). Lightning and precipitation history of a microburst-producing storm. *Geophysical Research Letters*, *15*(11), 1185–1188. https://doi.org/10.1029/gl015i011p01185

Hashino, T., Chiruta, M., Polzin, D., Kubicek, A., & Wang, P. K. (2014). Numerical simulation of the flow fields around falling ice crystals with inclined orientation and the hydrodynamic torque. *Atmospheric Research*, *150*, 79–96. https://doi.org/10.1016/j.atmosres.2014.07.003

Hayashi, S., Umehara, A., Nagumo, N., & Ushio, T. (2021). The relationship between lightning flash rate and ice-related volume derived from dual-polarization radar. *Atmospheric Research*, *248*, 105166. https://doi.org/10.1016/j.atmosres.2020.105166

Hendry, A., & McCormick, G. C. (1976). Radar observations of the alignment of precipitation particles by electrostatic fields in thunderstorms. *Journal of Geophysical Research*, *81*(30), 5353–5357. https://doi.org/10.1029/JC081i030p05353

Hubbert, J. C., & Bringi, V. N. (1995). An iterative filtering technique for the analysis of copolar differential phase and dual-frequency radar measurements. *Journal of Atmospheric and Oceanic Technology*, *12*(3), 643–648. https://doi.org/10.1175/1520-0426(1995)012<0643:AIFTFT>2.0.CO;2

Hubbert, J. C., Ellis, S. M., Chang, W. Y., & Liou, Y. C. (2014). X-band polarimetric observations of cross coupling in the ice phase of convective storms in Taiwan. *Journal of Applied Meteorology and Climatology*, *53*(6), 1678–1695. https://doi.org/10.1175/JAMC-D-13-0360.1

Hubbert, J. C., Ellis, S. M., Chang, W. Y., Rutledge, S., & Dixon, M. (2014). Modeling and interpretation of S-band ice crystal depolarization signatures from data obtained by simultaneously transmitting horizontally and vertically polarized fields. *Journal of Applied Meteorology and Climatology*, *53*(6), 1659–1677. https://doi.org/10.1175/JAMC-D-13-0158.1

Ishii, K., Hayashi, S., & Fujibe, F. (2014). Statistical analysis of temporal and spatial distributions of cloud-to-ground lightning in Japan from 2002 to 2008. *Journal of Atmospheric Electricity*, *34*(2), 79–86. https://doi.org/10.1541/jae.34.79

Krehbiel, P. R. (1986). The electrical structure of thunderstorms. In *The Earth's electrical environment* (pp. 90–113). National Academies Press.

Krehbiel, P. R., Chen, T., McCrary, S., Rison, W., Gray, G., Blackman, T., & Brook, M. (1992). Dual polarization radar signatures of the potential for lightning in electrified storms. In *9th International conference atmospheric electricity, St. Petersburg, Russia* (pp. 166–169).

Krehbiel, P. R., Chen, T., McCrary, S., Rison, W., Gray, G., & Brook, M. (1996). The use of dual channel circular-polarization radar observations for remotely sensing storm electrification. *Meteorology and Atmospheric Physics*, *59*(1–2), 65–82. https://doi.org/10.1007/BF01032001

Kuhlman, K. M., Ziegler, C. L., Mansell, E. R., MacGorman, D. R., & Straka, J. M. (2006). Numerically simulated electrification and lightning of the 29 June 2000 STEPS supercell storm. *Monthly Weather Review*, *134*(10), 2734–2757. https://doi.org/10.1175/MWR3217.1

Lang, T. J., Ahijevych, D. A., Nesbitt, S. W., Carbone, R. E., Rutledge, S. A., & Cifelli, R. (2007). Radar-observed characteristics of precipitating systems during NAME 2004. *Journal of Climate*, *20*(9), 1713–1733. https://doi.org/10.1175/JCLI4082.1

Latham, J., Petersen, W. A., Deierling, W., & Christian, H. J. (2007). Field identification of a unique globally dominant mechanism of thunderstorm electrification. *Quarterly Journal of the Royal Meteorological Society: A Journal of the Atmospheric Sciences, Applied Meteorology and Physical Oceanography*, *133*(627), 1453–1457. https://doi.org/10.1002/qj.133

Lhermitte, R., & Krehbiel, P. R. (1979). Doppler radar and radio observations of thunderstorms. *IEEE Transactions on Geoscience Electronics*, *17*(4), 162–171. https://doi.org/10.1109/TGE.1979.294644

Mattos, E. V., Machado, L. A., Williams, E. R., & Albrecht, R. I. (2016). Polarimetric radar characteristics of storms with and without lightning activity. *Journal of Geophysical Research: Atmospheres*, *121*(23), 14–201. https://doi.org/10.1002/2016JD025142

Mattos, E. V., Machado, L. A., Williams, E. R., Goodman, S. J., Blakeslee, R. J., & Bailey, J. C. (2017). Electrification life cycle of incipient thunderstorms. *Journal of Geophysical Research: Atmospheres*, *122*(8), 4670–4697. https://doi.org/10.1002/2016JD025772

McCormick, G. C., & Hendry, A. (1979). Radar measurement of precipitation-related depolarization in thunderstorms. *IEEE Transactions on Geoscience Electronics*, *17*(4), 142–150. https://doi.org/10.1109/TGE.1979.294641

Mecikalski, R. M., Bain, A. L., & Carey, L. D. (2015). Radar and lightning observations of deep moist convection across northern Alabama during DC3: 21 May 2012. *Monthly Weather Review*, *143*(7), 2774–2794. https://doi.org/10.1175/MWR-D-14-00250.1

Metcalf, J. I. (1992). *Radar observations of the effects of changing electric fields on the orientations of hydrometeors (No. 1100)*. Phillips Laboratory, Directorate of Geophysics.

Metcalf, J. I. (1995). Radar observations of changing orientations of hydrometeors in thunderstorms. *Journal of Applied Meteorology and Climatology*, *34*(4), 757–772. https://doi.org/10.1175/1520-0450(1995)034<0757:ROOCOO>2.0.CO;2

Noel, V., & Sassen, K. (2005). Study of planar ice crystal orientations in ice clouds from scanning polarization lidar observations. *Journal of Applied Meteorology and Climatology*, *44*(5), 653–664. https://doi.org/10.1175/JAM2223.1

Park, S. G., Bringi, V. N., Chandrasekar, V., Maki, M., & Iwanami, K. (2005). Correction of radar reflectivity and differential reflectivity for rain attenuation at X band. Part I: Theoretical and empirical basis. *Journal of Atmospheric and Oceanic Technology*, *22*(11), 1621–1632. https://doi.org/10.1175/JTECH1803.1

Park, S. G., Maki, M., Iwanami, K., Bringi, V. N., & Chandrasekar, V. (2005). Correction of radar reflectivity and differential reflectivity for rain attenuation at X band. Part II: Evaluation and application. *Journal of Atmospheric and Oceanic Technology*, *22*(11), 1633–1655. https://doi.org/10.1175/JTECH1804.1

Reynolds, S. E., & Brook, M. (1956). Correlation of the initial electric field and the radar echo in thunderstorms. *Journal of the Atmospheric Sciences*, *13*(4), 376–380. https://doi.org/10.1175/1520-0469(1956)013<0376:COTIEF>2.0.CO;2

Reynolds, S. E., Brook, M., & Gourley, M. F. (1957). Thunderstorm charge separation. *Journal of the Atmospheric Sciences*, *14*(5), 426–436. https://doi.org/10.1175/1520-0469(1957)014<0426:TCS>2.0.CO;2

Ryzhkov, A. V., & Zrnić, D. S. (2007). Depolarization in ice crystals and its effect on radar polarimetric measurements. *Journal of Atmospheric and Oceanic Technology*, *24*(7), 1256–1267. https://doi.org/10.1175/JTECH2034.1

Sassen, K. (1980). Remote sensing of planar ice crystal fall attitudes. *Journal of the Meteorological Society of Japanese Series II*, *58*(5), 422–429. https://doi.org/10.2151/jmsj1965.58.5_422

Saunders, C. P. R. (1993). A review of thunderstorm electrification processes. *Journal of Applied Meteorology and Climatology*, *32*(4), 642–655. https://doi.org/10.1175/1520-0450(1993)032<0642:AROTEP>2.0.CO;2

Saunders, C. P. R., Bax-Norman, H., Emersic, C., Avila, E. E., & Castellano, N. E. (2006). Laboratory studies of the effect of cloud conditions on graupel/crystal charge transfer in thunderstorm electrification. *Quarterly Journal of the Royal Meteorological Society: A Journal of the Atmospheric Sciences, Applied Meteorology and Physical Oceanography*, *132*(621), 2653–2673. https://doi.org/10.1256/qj.05.218

Saunders, C. P. R., Keith, W. D., & Mitzeva, R. P. (1991). The effect of liquid water on thunderstorm charging. *Journal of Geophysical Research*, *96*(D6), 11007–11017. https://doi.org/10.1029/91JD00970

Saunders, C. P. R., & Rimmer, J. S. (1999). The electric field alignment of ice crystals in thunderstorms. *Atmospheric Research*, *51*(3–4), 337–343. https://doi.org/10.1016/S0169-8095(99)00018-6

Schneebeli, M., Dawes, N., Lehning, M., & Berne, A. (2013). High-resolution vertical profiles of X-band polarimetric radar observables during snowfall in the Swiss Alps. *Journal of Applied Meteorology and Climatology*, *52*(2), 378–394. https://doi.org/10.1175/JAMC-D-12-015.1

Schvartzman, D., Bruning, E., Yu, T. Y., Chmielewski, V., Bodine, D., & Bluestein, H. B. (2022). Analysis of polarimetric spectral densities in severe thunderstorms for the identification of lightning-induced signatures.

Scott, R. D., Krehbiel, P. R., & Rison, W. (2001). The use of simultaneous horizontal and vertical transmissions for dual-polarization radar meteorological observations. *Journal of Atmospheric and Oceanic Technology*, *18*(4), 629–648. https://doi.org/10.1175/1520-0426(2001)018<0629:TUOSHA>2.0.CO;2

Shackford, C. R. (1960). Radar indications of a precipitation-lightning relationship in New England thunderstorms. *Journal of the Atmospheric Sciences*, *17*(1), 15–19. https://doi.org/10.1175/1520-0469(1960)017<0015:RIOAPL>2.0.CO;2

Stolzenburg, M., Rust, W. D., & Marshall, T. C. (1998). Electrical structure in thunderstorm convective regions 2. Isolated storms. *Journal of Geophysical Research*, *103*(D12), 14079–14096. https://doi.org/10.1029/97JD03547

Stolzenburg, M., Rust, W. D., Smull, B. F., & Marshall, T. C. (1998). Electrical structure in thunderstorm convective regions: 1. Mesoscale convective systems. *Journal of Geophysical Research*, *103*(D12), 14059–14078. https://doi.org/10.1029/97JD03546

Takahashi, T. (1978). Riming electrification as a charge generation mechanism in thunderstorms. *Journal of the Atmospheric Sciences*, *35*(8), 1536–1548. https://doi.org/10.1175/1520-0469(1978)035<1536:REAACG>2.0.CO;2

Tessendorf, S. A., Rutledge, S. A., & Wiens, K. C. (2007). Radar and lightning observations of normal and inverted polarity multicellular storms from STEPS. *Monthly Weather Review*, *135*(11), 3682–3706. https://doi.org/10.1175/2007MWR1954.1

Testud, J., Le Bouar, E., Obligis, E., & Ali-Mehenni, M. (2000). The rain profiling algorithm applied to polarimetric weather radar. *Journal of Atmospheric and Oceanic Technology*, *17*(3), 332–356. https://doi.org/10.1175/1520-0426(2000)017<0332:TRPAAT>2.0.CO;2

Timothy, L., Brenda, D., Nick, G., CAM, G., & Joseph, H. (2019). CSU-Radarmet/CSU_RadarTools: CSU_RadarTools v1.3 (version 1.3) [Software]. *Zenodo*. https://doi.org/10.5281/zenodo.2562063

Ushio, T., Heckman, S. J., Boccippio, D. J., Christian, H. J., & Kawasaki, Z. I. (2001). A survey of thunderstorm flash rates compared to cloud top height using TRMM satellite data. *Journal of Geophysical Research*, *106*(D20), 24089–24095. https://doi.org/10.1029/2001JD900233

Ventura, J. F., Honoré, F., & Tabary, P. (2013). X-band polarimetric weather radar observations of a hailstorm. *Journal of Atmospheric and Oceanic Technology*, *30*(9), 2143–2151. https://doi.org/10.1175/JTECH-D-12-00243.1

Vivekanandan, J., Zrnić, D. S., Ellis, S. M., Oye, R., Ryzhkov, A. V., & Straka, J. (1999). Cloud microphysics retrieval using S-band dual-polarization radar measurements. *Bulletin of the American Meteorological Society*, *80*(3), 381–388. https://doi.org/10.1175/1520-0477(1999)080<0381:CMRUSB>2.0.CO;2

Wang, S. (2023a). Electrical alignment signatures of ice particles before intracloud lightning activity detected by dual-polarized phased array weather radar (version 1) [Dataset]. *Zenodo*. https://doi.org/10.5281/zenodo.8409201

Wang, S. (2023b). Observation of electrical alignment signatures in an isolated thunderstorm by dual-polarized phased array weather radar and the relationship with intracloud lightning flash rate [Dataset]. *Zenodo*. https://doi.org/10.5281/zenodo.10429831

Wang, S., Wada, Y., Hayashi, S., Ushio, T., & Chandrasekar, V. (2024). Electrical alignment signatures of ice particles before intracloud lightning activity detected by dual-polarized phased array weather radar. *Journal of Geophysical Research: Atmospheres*, *129*(7), e2023JD039942. https://doi.org/10.1029/2023JD039942

Weinheimer, A. J., & Few, A. A. (1987). The electric field alignment of ice particles in thunderstorms. *Journal of Geophysical Research*, *92*(D12), 14833–14844. https://doi.org/10.1029/JD092iD12p14833

Wiens, K. C., Rutledge, S. A., & Tessendorf, S. A. (2005). The 29 June 2000 supercell observed during STEPS. Part II: Lightning and charge structure. *Journal of the Atmospheric Sciences*, *62*(12), 4151–4177. https://doi.org/10.1175/JAS3615.1

Williams, E. R. (1981). *Thunderstorm electrification: Precipitation versus convection, Ph.D. thesis*. Massachusetts Institute of Technology.

Williams, E. R. (1985). Large-scale charge separation in thunderclouds. *Journal of Geophysical Research*, *90*(D4), 6013–6025. https://doi.org/10.1029/JD090iD04p06013

Williams, E. R. (1989). The tripole structure of thunderstorms. *Journal of Geophysical Research*, *94*(D11), 13151–13167. https://doi.org/10.1029/jd094id11p13151

Williams, E. R. (2001). The electrification of severe storms. In *Severe convective storms* (pp. 527–561). American Meteorological Society.

Workman, E. J., & Reynolds, S. E. (1949). Electrical activity as related to thunderstorm cell growth. *Bulletin of the American Meteorological Society*, *30*(4), 142–144. Retrieved from https://www.jstor.org/stable/26258148

Zipser, E. J., & Lutz, K. R. (1994). The vertical profile of radar reflectivity of convective cells: A strong indicator of storm intensity and lightning probability? *Monthly Weather Review*, *122*(8), 1751–1759. https://doi.org/10.1175/1520-0493(1994)122<1751:TVPORR>2.0.CO;2

Zrnić, D. S., & Ryzhkov, A. V. (1999). Polarimetry for weather surveillance radars. *Bulletin of the American Meteorological Society*, *80*(3), 389–406. https://doi.org/10.1175/1520-0477(1999)080<0389:PFWSR>2.0.CO;2